Journal of Inorganic and Organometallic Polymers and Materials (2024) 34:1150–1171
https://doi.org/10.1007/s10904-023-02872-w

RESEARCH

Efficacious Recovery of Zirconium and Yttrium Ions from Effluents Using a Gamma-Irradiated Reduced Graphene Oxide Polymeric Composite

Ahmed Atef Eliwa[1]

Received: 20 August 2023 / Accepted: 12 September 2023 / Published online: 6 October 2023

Abstract
There are many great uses for heavy elements that are expanding daily and generating enormous amounts of effluents. Therefore, tremendous scientific efforts in removing, recovering, and recycling them are carried out to prevent these harmful effects on the environment and human health. The polyacrylic-carboxymethyl cellulose-trioctyl amine/reduced graphene oxide adsorbent (AA-CMC-TOA/rGO) was synthesized as a promising sorbent for Zr^{4+} and Y^{3+} ions by gamma irradiation for a mixture of acrylic acid, carboxymethyl cellulose, and trioctyl amine as an organic solvent. A complete characterization of the manufactured composite was carried out to find out its chemical and physical properties several techniques such as XRD, EDX, SEM, FT-IR, TGA-DTA, and BET. Several factors affecting the Zr^{4+} and Y^{3+} adsorption processes were studied to set the best conditions that achieve the extreme loading capacity of Zr^{4+} and Y^{3+} ions. Loading capacities of 0.99 and 1.07 mmol g^{-1} were achieved for Zr^{4+} and Y^{3+}, respectively. The results of the kinetic models indicated that the adsorption reactions of Zr^{4+} and Y^{3+} ions were carried out via a chemical reaction mechanism. Langmuir, Dubinin–Radushkevich, and Redlich–Peterson models accurately described the adsorption isotherm data by proving their chemical nature. The results of thermodynamics added evidence of the chemical nature, spontaneous, and endothermic nature of the adsorption processes. A complete retrieval for Zr^{4+} and Y^{3+} ions contents located in the effluent was efficiently achieved using AA-CMC-TOA/rGO sorbent which proved its uses as a promising sorbent.

Keywords Trioctyl amine · Reduced graphene oxide · Adsorption · Zirconium (IV) · Yttrium (III)

1 Introduction

Yttrium and zirconium are chemical elements of about 31 and 130 mg kg^{-1} within the Earth's crust and about 0.009 and 0.026 µg L^{-1} in seawater making them the 17th and 28th most abundant element respectively [1, 2]. The silver-colored yttrium was considered a transition metal; it was chemically similar to the lanthanides and was classified as a rare-earth element [3]. Yttrium has always been observed in combination with the lanthanide elements in rare earth minerals and has not been observed alone in nature. Yttrium compounds have numerous applications as their uses as garnets, material enhancers, medical, superconductors, and Lithium batteries [4–6]. On the other hand, Zirconium, a lustrous element with gray-white colors, was an important element with unique properties, being a strong transition metal very similar to hafnium and to a lesser extent similar to titanium. Zirconium has many uses such as its use as a refractory and a pacifier. Relatively small amounts of zirconium were added to alloys to improve their properties and enhance corrosion resistance. Zirconium compounds and alloys have wide applications, especially in nuclear, space, aeronautic, defunct, and medical applications [7].

Fifty kinds of rare earth minerals have been used industrially in the production technology of rare earth elements. Only 10 of them were used industrially and commercially to yield rare earth, namely xenotime, monazite, bastnaesite, fergusonite, Ion-absorbed-type, euxenite, allanite, and gadolinite [8, 9]. On the other hand, zircon ($ZrSiO_4$), which was a silicate mineral, was found in smaller deposits around the world and was the essential commercial provenance of zirconium [10]. Currently, the traditional industrial processes

✉ Ahmed Atef Eliwa
aaaliwa@yahoo.com

[1] Semi-Pilot Plant Department, Nuclear Materials Authority, El-Maadi, Cairo, Egypt

used in rare-earths production and high-purity zirconium have been characterized by bad effects on the environment. Huge amounts of volatile organic compounds and chemical wastes were released resulting in water and air pollution [11]. Therefore, several researchers have developed eco-friendly technologies for the production of rare elements and zirconium. Globally separation techniques based on solvent extraction and ion exchange were used to produce high-purity oxides of Zr^{4+} and Y^{3+} ions [12–17]. Nowadays, there were extensive studies on the use of adsorption technology on solid surfaces as a technology more suitable for widespread use due to its simplicity, low cost, as well as high performance compared to other technologies. Sorbents can be broadly categorized into inorganic sorbents, organic sorbents, and bio-sorbents [18, 19]. Natural and synthetic zeolites, activated carbon, clay minerals, and resins have been used as sorbent materials.

Numerous hydrometallurgical treatments for rare-earths bearing minerals such as xenotime, monazite, samarskite, and fergusonite as well as for zirconium-bearing minerals such as zircon, were carried out in the specialized laboratories of the Egyptian Nuclear Materials Authority (NMA) [10, 20–22]. After completing various recoveries of the desired elements, this resulted in large amounts of effluent containing varying concentrations of Y^{3+} and Zr^{4+} ions. Therefore, the production of materials, which were characterized by ease of use and high efficiency of assimilation of these elements, was required to recover metal ions from other polluting elements. The maintenance of the physical and chemical resistance and high stability of these manufactured compounds when mixed with various acidic media was also required. Finally, the simplicity of synthesis and low cost were the main requirements for such innovations in the manufacture of adsorbents.

Due to the prodigious constancy of organometallic complexes, there were many studies on the possibility of extracting mineral ions by organic composites [23]. Many organic polymers, which have high chemical stability and homogeneity, were rarely used as adsorbents due to poor mechanical strength, such as poly-acrylic acid, poly-acrylamide, and poly-malic acid. Therefore, several studies have been done on enhancing their mechanical strength by combining them with other compounds [24]. During this study, several compounds were combined, such as tertiary amines, carboxymethylcellulose with multiple functional properties, and graphene reducing oxide as a supporting material in order to obtain a successful resin in the extraction processes of both elements. All these organic contents contained many functional groups that were able to interact successfully with the studied metal ions. As a consequence of the use of quaternary ammonium salts, especially those with a long chain, on a commercial scale for the extraction of yttrium ions in pure form as well as the successful use of Tri-octyl amine(TOA) for the extraction of zirconium in several previous studies [25, 26], it was decided to use TOA by binding and merging with some other organic polymers, which reduces the chances of significant consumption in the organic content during its use as an organic solvent, which was considered a negative factor and reduced the possibility of its use before [22]. On the other hand, the addition of graphene or reduced graphene oxide to polymeric materials can improve their appropriate mechanical, thermal and chemical relationships, and their specific surface area [27–29].

Therefore, the main objective of the research was to study the possibility of recovering Zr^{4+} and Y^{3+} ions from an effluent solution obtained and synthesized in the laboratories of the Egyptian Nuclear Materials Authority for reuse in other applications in the future. New material was synthesized by polymerizing a mixture of organic materials by irradiation technique to obtain a physically and chemically distinct resin, which was polyacrylic-carboxymethyl cellulose-trioctylamine/reduced graphene oxide adsorbent (AA-CMC-TOA/rGO). The manufactured material has been described using FTIR, XRD, SEM, TGA-DTA, BET and EDX. Furthermore, various factors influencing the adsorption process of the two elements, such as the feed solution pH, the reaction time, the reaction temperature, the dose of sorbent, the concentrations of metal ions, and the competing elements' impacts, were scrutinized to define the best adsorption parameters. Adsorption kinetics, isotherms, and thermodynamics were studied with the aim of getting an authentic comprehension of the adsorption mechanism, its nature, and its properties.

2 Materials and Methods

2.1 Reagents and Materials

Zirconium oxychloride ($ZrOCl_2{\cdot}8H_2O$) and yttrium oxide (Y_2O_3) were used as Zr^{4+} and Y^{3+} ion sources and were purchased from Sigma-Aldrich. Acrylic acid (AA) with a purity of 99%, a monomer, was purchased from ATOFINA Chemical Co. Food Chem Co., USA supplied the sodium carboxymethyl cellulose (CMC). Fluka supplied the anionic extractant TOA, and Merck (Germany) provided the methylene bis-acrylamide (MBA) cross-linker and graphite powders. The ascorbic acid was gained from the Egyptian Bratachem. Co. Throughout this study, double distilled water (DDW) was used. Hydrochloric acid (HCl), Sulfuric acid (H_2SO_4), and sodium hydroxide (NaOH), which were used throughout this study in the pH adjustments and regeneration, were attained from Merck. For the batch sorption studies, zirconium oxychloride and yttrium oxide were completely dissolved in sulfuric acid, and diluted to the proper concentrations. The precipitation limits of Zr^{4+} and Y^{3+} ions were taken into consideration and determined

to avoid sedimentation caused by increasing the pH value. This could eliminate the confusion between the deposition of metal ions at high pH values and their adsorption on the AA-CMC-TOA/rGO adsorbent surface.

2.2 Synthesis of AA-CMC-TOA/rGO Sorbent

Reduced graphene oxide (rGO) was prepared through the reduction of graphene oxide (GO) synthesized by the Hummer process in the Nuclear Chemistry Department lab at the Egyptian Atomic Energy Authority. Free radical polymerization technique was used in the preparation of AA-CMC-TOA/rGO sorbent. Ascorbic acid was used as an oxidizing agent. 50 mL of distilled water was used to dissolve 3.5 g of carboxymethyl cellulose, and 3.5 mL of acrylic acid was added, along with 2 mL of TOA. After stirring the initial mixture for 30 min, 1 g of rGO and 0.05 mg of MBA as cross-linker were added. The entire mixture was vigorously stirred for 24 h. The mixture was irradiated with 25 kGy rays in a cobalt-60 gamma cell in the cyclotron project of the Egyptian Atomic Energy Authority. After irradiation, the prepared materials were reduced into small parts and drenched in acetone for 2 h to eliminate water and contaminants. The soaked parts were dried in a vacuum oven at 333 K for 24 h, milled in an electric grinder, and sieved to the proper size (200–300 µm).

2.3 Instrumentation and Characterization

To recognize the functional groups present on the AA-CMC-TOA/rGO sorbent, a FTIR spectrophotometer (Bomen Mickelson), model MB157, Canada, was used using Fourier transform infrared (FT-IR). Evaluating the crystalline construction of the synthesized composite was performed using X-ray diffraction (XRD), Shimadzu, model XD-Dl from Kyoto, Japan. Investigating the phase and mass variations was carried out from 46 to 650 °C using a DTA-TGA system of type DTA-TGA-50, Japan. The sorbent constituents and their morphology were inspected using the scanning electron micrograph model JEOL-JSM-5600LV (FEI Quanta FEG-250, EDX), JEOL LTD from Japan. The BET surface area, the pore size distribution, and N_2 adsorption–desorption isotherms of the AA-CMC-TOA/rGO composite were determined using a surface area analyzer (Nova 3200 series, Micrometric) (USA). The concentrations of Zr^{4+}, Y^{3+}, Ti^{4+}, Nb^{5+}, Fe^{3+}, and Ca^{2+} were determined using the appropriate spectrophotometric methods using UV-spectrophotometer model SP-8001, Metretech Inc, china [30]. The Na^{+} ions concentration was identified using a Sherwood Scientific Flame Photometer Model 410, UK.

2.4 Adsorption Batch Experiments

To investigate the potentiality and the sorption behavior of Zr^{4+} and Y^{3+} ions on AA-CMC-TOA/rGO sorbent, several parameters were studied. 10 mL feed portions containing definite concentrations from Zr^{4+} and Y^{3+} ions each separately were mixed with 0.01 g prepared sorbent in 50 mL glass flask bottles and stirred for a definite period of minutes with 300 rpm. Several parameters were studied to optimize the sorption processes of both metal ions. Aqueous phase pH, sorption time, metal ion concentrations, and sorbent dose impacts were studied. During all experiments and after the stirring time has elapsed, the decantation and filtration processes were carried out to remove the solid sorbent and measure the concentrations of both elements remaining in the filtrate. Through Eqs. (1–3), the sorption capacities and efficiencies of both metal ions were identified.

$$\text{Sorption efficiency}(\%) = \left(\frac{C_0 - C_e}{C_0}\right) \times 100 \tag{1}$$

$$q_t = \left(C_o - C_t\right) \times \frac{V}{m} \tag{2}$$

$$q_e = \left(C_o - C_e\right) \times \frac{V}{m} \tag{3}$$

where q_e and q_t (mmol g^{-1}), were the Zr^{4+} and Y^{3+} ions quantities on the composite at the equilibrium time and at the adsorption time t (min), respectively. The C_o and C_e (mmol L^{-1}) were the initial metal ion concentrations and their concentrations at equilibrium respectively. Moreover, C_t indicated the metal ions concentrations existing in the aqueous phase at adsorption time t. V and m characterized the volume (L) of the feed solution, and the mass of the solid sorbent (g) respectively.

Each test was repeated three times to calculate the averaged findings using the standard deviation. The competing ions' impact was studied extensively using a certain concentration of one of the coexisting elements Na^{+}, Ca^{2+}, Fe^{3+}, Ti^{4+}, and Nb^{5+} ions. A definite content from Zr^{4+} or Y^{3+} ions was mixed with equal content from the competing metal ions and the competing experiments were performed using the optimal operating conditions that have been achieved through previous experiments. The studied factors affecting the adsorption process, as well as the extent of change in these factors, and the other fixed conditions during the study of each influencing factor were collected in Table 1.

Table 1 The sorption parameters of Zr^{4+} and Y^{3+} ions on the AA-CMC-TOA/rGO sorbent

Sorption parameters	Extent of change	Stable conditions
pH	1– 2.3 for Zr^{4+} 1–5 for Y^{3+}	0.01 g resin, 10 mL liquid, 0.99 mmol L^{-1} Zr^{4+} or 1.07 mmol L^{-1} Y^{3+}, 298 K, 60 min
Sorbent dose, g	0.01–0.05	10 mL liquid, 0.99 mmol L^{-1} Zr^{4+} or 1.07 mmol L^{-1} Y^{3+}, 298 K, pH = 2 for Zr^{4+} and 4.0 for Y^{3+}, 45 min
Metal ion conc., mmol L^{-1}	0.27–2.20 for Zr^{4+} 0.28–2.25 for Y^{3+}	0.01 g resin, 10 mL liquid, 298 K, pH = 2 for Zr^{4+} and 4.0 for Y^{3+}, 45 min
Stirring temp., K	298–323	0.01 g resin, 10 mL liquid, 0.99 mmol L^{-1} Zr^{4+} or 1.07 mmol L^{-1} Y^{3+} pH = 2 for Zr^{4+} and 4.0 for Y^{3+}, 45 min
Competing ions	Na^{+}, Ca^{2+}, Fe^{3+}, Ti^{3+}, and Nb^{3+}	0.01 g resin, 10 mL liquid, 0.99 mmol L^{-1} Zr^{4+} or 1.07 mmol L^{-1} Y^{3+}, equal conc. from competing ions 298 K, pH = 2 for Zr^{4+} and 4.0 for Y^{3+}, 45 min

2.5 Adsorption Isotherms, Kinetics, and Thermodynamics

2.5.1 Adsorption Isotherm Modeling

Langmuir [31], Freundlich [31], Redlich–Peterson [32], and Dubinin–Radushkevich (D-R) isotherms [31] were applied through this work to give vision into the sorption mechanisms and the composite surface properties. Equations (4–7) investigated the non-linear adsorption isotherm modeling forms. Equation (4) was Langmuir nonlinear form; Eqs. (5) and (6) were for Freundlich and Redlich–Peterson nonlinear form, respectively. Equation (7) was used for non-linear regression of Dubinin–Radushkevich (D-R) isotherm. Equation (8) was the equation used to calculate the value of the activation energies of the absorption processes of both elements the results obtained from (D-R) isotherm.

$$q_e = \frac{q_m K_L C_e}{1 + K_L C_e} \tag{4}$$

$$q_e = K_F C_e^{1/n} \tag{5}$$

$$q_e = \frac{K_{RP} C_e}{1 + a_{RP} C_e^{B}} \tag{6}$$

$$q_{mDR} = e^{-\beta_{DR}\varepsilon^2} \tag{7}$$

$$E = \frac{1}{\sqrt{2\beta}} \tag{8}$$

where q_m (mmol g^{-1}) was the monolayer sorption capacity; K_L (L mg^{-1}) was constant related to the free energy of adsorption. K_f denoted Freundlich constants and n denoted sorption capacity and intensity. K_{RP}, a_{RP}, and B ($0 < B < 1$) were three constants related to Redlich–Peterson Isotherm. q_{mDR} was the monolayer capacity for the D-R model, β_{DR} was a constant related to apparent adsorption energy, ε was Polanyi potential. Langmuir adsorption isotherm describes the solute sorption onto sorbents as monolayer adsorption onto homogeneous active sites. Freundlich isotherm describes multilayer adsorption onto heterogeneous surfaces with the interaction between adsorbed molecules. The Redlich–Peterson isotherm also includes the features of Langmuir and Freundlich isotherms and can be applied to either homogeneous or heterogeneous systems [32]. If the value of B was close to unity, the isotherm approaches Langmuir, otherwise it approaches Freundlich.

2.5.2 Adsorption Kinetic Modeling

The sorption rate determination step for Zr^{4+} and Y^{3+}onto AA-CMC-TOA/rGO sorbent and the order of their reactions could be described by applying pseudo-1st-order, pseudo-2nd-order, Elvoich, and pseudo-nth-order kinetic models.

Pseudo-1st-order and Pseudo-2nd -order:

Pseudo-1.st-order kinetics applied using the non-linear form as shown in Eq. (9)

$$q_t = q_{e(cal.)}\left(1 - e^{-k_1 t}\right) \tag{9}$$

Equation (10) was the non-linear form of the pseudo-2nd-order model

$$q_t = \left(\left(k_2 q_{e(cal.)}^2 t\right) / \left(1 + k_2 q_e t\right)\right) \tag{10}$$

where K_1 was the pseudo-1st-order rate constant. q_t and $q_{e(cal.)}$ were the sorbed amounts at time t and at equilibrium respectively. K_2 denoted the pseudo-2nd-order kinetic constant [33, 34].

Elvoich model:

The Elvoich model was taken as evidence of the compatibility of the chemisorption reaction with second-order kinetics. The non-linear form of the Elvoich model could be represented by Eq. (11).

$$q_t = 1/\beta \ln(1 + \alpha\beta t) \quad (11)$$

where α and β were the Elovich constants. α was the Elovich initial adsorption rate (mg g^{-1} min) and β was the desorption constant (g mg^{-1}) [31].

Pseudo-nth-order:

The kinetic analysis was not limited to pseudo-1st-order or pseudo-2nd-order. Pseudo-nth-order Eq. (12) was hence suggested for multistep reactions or complex mechanisms [22].

$$\frac{q_t}{q_e} = 1 - \frac{1}{\left[1 + (n-1)q_e^{n-1}k_n t\right]^{\left(\frac{1}{n-1}\right)}} \quad (12)$$

where K_n was the pseudo-nth-order rate constant (kg^{n-1} g^{1-n} min^{-1}), n was the order of reaction and it could be a fraction or an integral number.

2.5.3 Thermodynamics Studies

Thermodynamic studies of the adsorption processes of Zr^{4+} and Y^{3+} ions on the AA-CMC-TOA/rGO composite were investigated using the temperature factor outcomes. The enthalpy and entropy changes for the sorption processes were calculated using the Van't Hoff equation (Eq. 13) [35]. The Gibbs free energy changes of the adsorption processes were calculated using Eq. (14).

$$\ln K_d = \frac{\Delta S^o}{R} - \frac{\Delta H^o}{RT} \quad (13)$$

$$\Delta G = \Delta H - T\Delta S \quad (14)$$

where ΔH^o (kJ mol^{-1}), ΔS^o (kJ mol K^{-1}), and ΔG_o (kJ mol^{-1}) were enthalpies, entropy changes, and Gibbs free energy changes, respectively. R (J K^{-1} mol^{-1}) and T (K) were the gas constant and the temperature.

Among quantitative error functions, the coefficient of determination R^2 and chi-square (χ^2) were determined for the resulting modeling data in order to determine the best-fit model for the sorption process. The best-fit model has a maximum value of R^2 (near to the unity) and a minimum value of χ^2. Equations (15, 16) represented the two equations used to determine the R^2 and χ^2 respectively [36].

$$R^2 = 1 - \frac{\sum_{i=1}^{n}\left(q_{calc.} - q_{exp.}\right)^2}{\sum_{i=1}^{n}\left(q_{calc.} - q_{mean}\right)^2} \quad (15)$$

$$x^2 = \sum \frac{\left(q_{calc.} - q_{exp.}\right)^2}{q_{calc.}} \quad (16)$$

where $q_{exp.}$, $q_{calc.}$, and q_{mean} (mmol g^{-1}) were the quantity of ions sorbed, the projected amount of sorbed ions, and the mean of $q_{exp.}$ values of ions respectively.

2.6 Desorption Studies and Application on a Real Effluent

The desorption processes of Zr^{4+} and Y^{3+} ions from the loaded AA-CMC-TOA/rGO sorbent were investigated to select the most appropriate eluent. These studies were performed by mixing the loaded sorbent with sulfuric and hydrochloric acids of two variable concentrations 0.5 and 1.0 mol L^{-1}. Desorption experiments were performed under several stationary conditions such as 0.5 g loaded sorbent, 5 mL acid solution, stirring for 45 min under 300 rpm at room temperature. After the end of each experiment, the spent AA-CMC-TOA/rGO sorbent was filtered and the remaining filtrate solution was analyzed to find out the Zr^{4+} and Y^{3+} ions contents as well as to determine their elution efficiencies according to Eq. (17).

$$Desorption\ efficiency = \left(\frac{C_e}{C_L}\right) \times 100 \quad (17)$$

where C_e and C_L were the concentrations of Zr^{4+} and Y^{3+} metal ions within the aqueous phase and on the adsorbent, respectively.

At the Nuclear Materials Authority's research facilities at the Inshas site in Egypt, laboratory solutions were collected as liquid waste. The effluent still contained respectable concentrations of Zr^{4+} and Y^{3+} ions as well as other contaminating metal ions present in these solutions. As a result, the effectiveness of the AA-CMC-TOA/rGO composite was evaluated using it to recover each of the studied elements from these real solutions as well as examining the competing elements' impact on the adsorption efficiencies of Zr^{4+} and Y^{3+} ions on AA-CMC-TOA/rGO composite and testing its selectivity.

3 Results and Discussion

3.1 Characteristics of the AA-CMC-TOA/rGO Sorbent

3.1.1 XRD Results

Figure 1 presented the X-ray diffraction analysis of the AA-CMC-TOA/rGO adsorbent. From the XRD pattern of the composite, an amorphous structure emerged revealing no evidence of a crystalline structure of the synthesized sorbent. It was preferable to use amorphous adsorbent over crystalline adsorbent in the processes of removing elemental ions and other solutions it carries because of the rapid diffusion of the solution through the adsorbent, the weak resistance to the flow of the solution, and the easy penetration between the layers [37]. As a result, this amorphous substance was

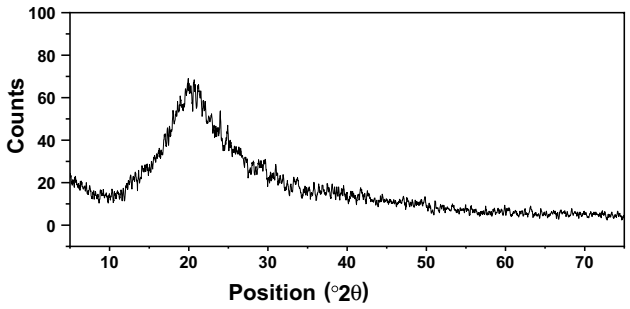

Fig. 1 XRD pattern of the AA-CMC-TOA/rGO sorbent

regarded as a helpful agent in experiments on the recovery of zirconium and yttrium ions, and the sharp peak that formed in a curve at 22° may be linked to the existence of rGO as a structural element in the adsorbent [38].

3.1.2 EDX Results

As shown in Fig. 2a, carbon, oxygen and nitrogen were the main elements which can be clearly seen in the EDX chart of manufactured sorbents. However, in the loaded sorbents shown in Fig. 2b, c, the C, N, and O percentages were clearly decreased as a result of the pronounced appearance of Zr^{4+} and Y^{3+} elements proving their uploading on the composite surface. Also, a rare appearance of undesirable elements such as sulfur and sodium were observed as a result of their presence in acidic solutions, on which

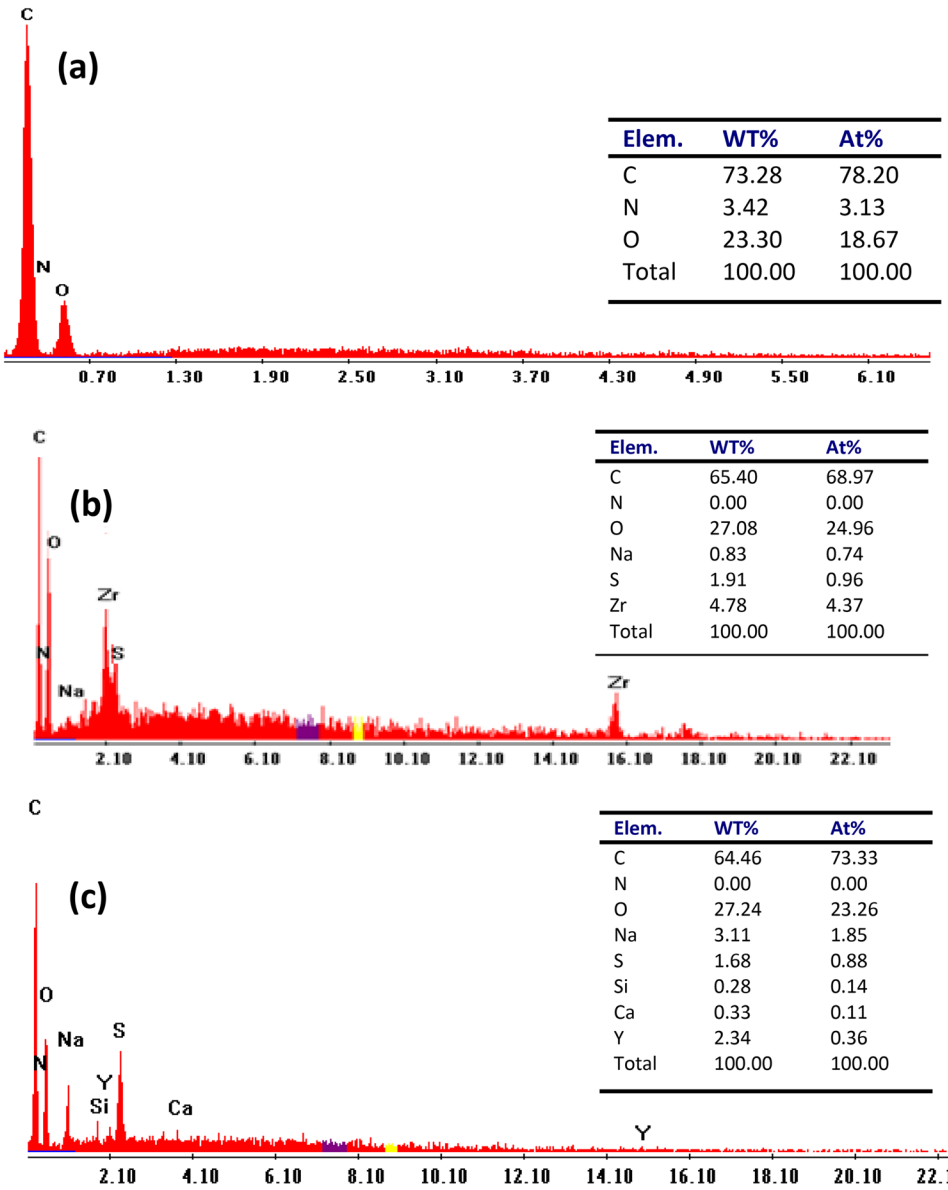

Elem.	WT%	At%
C	73.28	78.20
N	3.42	3.13
O	23.30	18.67
Total	100.00	100.00

Elem.	WT%	At%
C	65.40	68.97
N	0.00	0.00
O	27.08	24.96
Na	0.83	0.74
S	1.91	0.96
Zr	4.78	4.37
Total	100.00	100.00

Elem.	WT%	At%
C	64.46	73.33
N	0.00	0.00
O	27.24	23.26
Na	3.11	1.85
S	1.68	0.88
Si	0.28	0.14
Ca	0.33	0.11
Y	2.34	0.36
Total	100.00	100.00

Fig. 2 **a** EDX charts of the AA-CMC-TOA/rGO sorbent before adsorption, **b** EDX-chart after Zr^{4+} adsorption, and **c** EDX-chart after Y^{3+} adsorption

adsorption processes were performed, which indicated the probability of their adsorption along with the desired elements. The moderate appearance of the two metal ions as shown in Fig. 2b, c indicated the average ability of the resin to adsorb both Zr^{4+} and Y^{3+} ions. This could be attributed to the presence of both metal ions in polyvalent positive ions. However, all the functional groups presence on the resin skeleton were monovalent groups such as carboxylic (–COOH), hydroxyl (−OH), and amine (−NH). This means that the polyvalent zirconium and yttrium ions were necessary to bind with more than one active site to achieve equilibrium. This indicated a relatively low presence of both elements when compared to the C and O contents in the EDX analysis.

3.1.3 Morphology Results

As illustrated in Fig. 3, using two different drawing scales, the particles randomly assembled to form large agglomerations of heterogeneous shapes and a non-uniform size range in diameter. Due to the high cross-linking density and the presence of polymeric interactions with the TOA solvent, a rough and irregular surface with an overall variety of particle distribution appeared for AA-CMC-TOA/rGO adsorbent using SEM instrumental analysis [39, 40]. A lot of random corrugated cavities and cracks were observed in the compound before and after adsorption processes. Before the adsorption processes, the composite appeared without any white particles scattered on its surface. After the adsorption

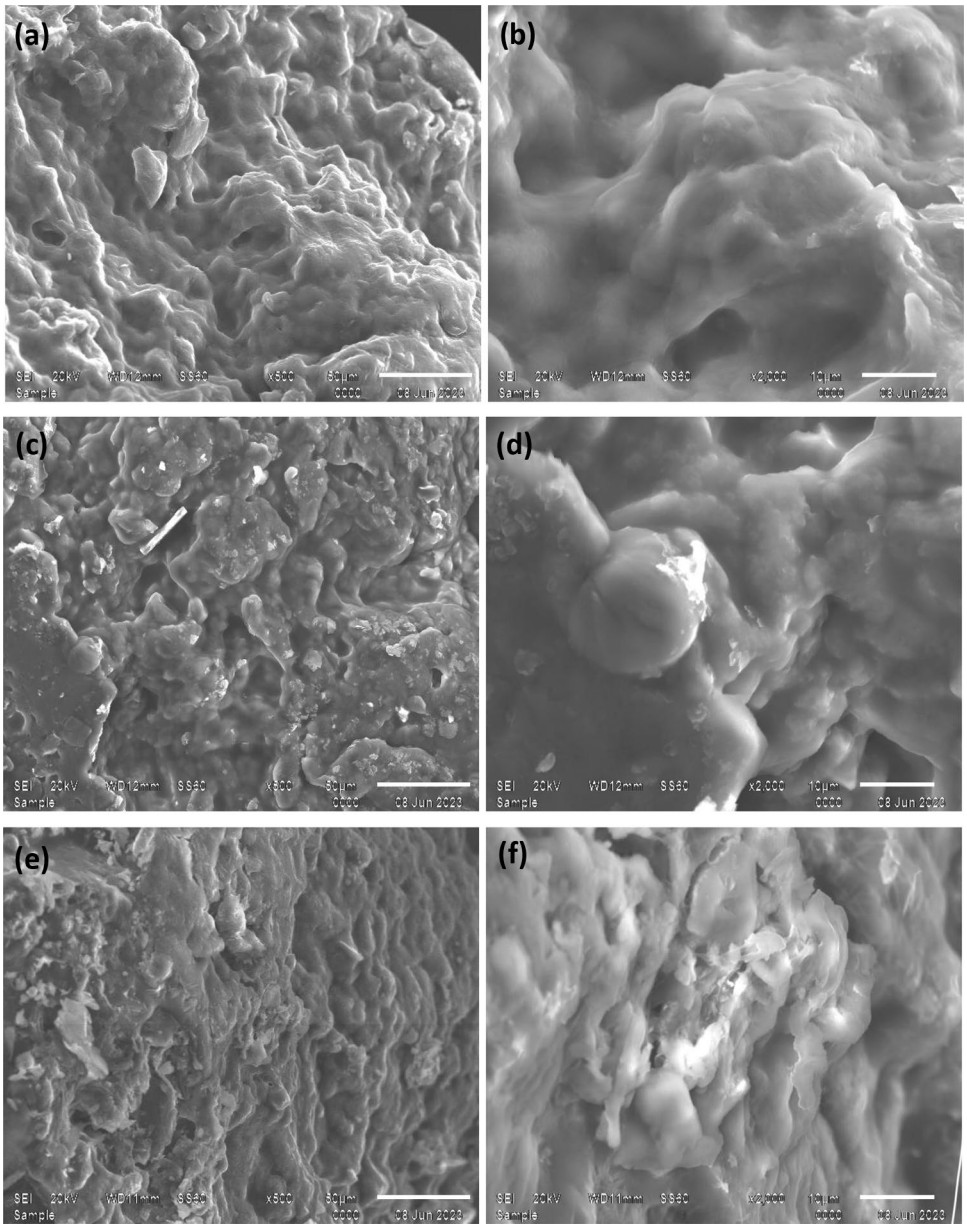

Fig. 3 **a**, **b** SEM-images of the AA-CMC-TOA/rGO sorbent, **c**, **d** AA-CMC-TOA/rGO-Zr, and **e**, **f** AA-CMC-TOA/rGO-Y

processes occurred, white particles appeared on the surface of the manufactured adsorbent, which proved the actual occurrence of adsorption processes and the entrapping of the recovered ions across the active sites of the AA-CMC-TOA/rGO sorbent. From Fig. 3c–f, after the adsorption of Zr^{4+} and Y^{3+} ions, the surface assumed a wave-like layered construction with a noticeable lack of interstitial voids, which were visibly reduced on the extrinsic surface owing to the adsorption of Zr^{4+} and Y^{3+} ions.

3.1.4 FTIR Results

FT-IR spectroscopy was considered one of the greatest significant methods of chemical analysis, where the functional groups and various bonds of the studied compound were monitored, and then the expected composition of the manufactured compound was proved. The FT-IR chart of the AA-CMC-TOA/rGO sorbent before and after the absorption of Zr^{4+} and Y^{3+} ions were shown in Fig. 4. The three composites were very similar while showing distinctive banding with some differences. First of all, the decrease in the intensity of the bands of the representative functional groups as well as the increase in the intensity of the metal ions-active sites interaction bands (M–O) indicated the adsorption of Zr^{4+} and Y^{3+} on the composite adsorbent. The resulting spectrum of the manufactured resin was divided into three distinct zones. The first region was the high-energy bands, which ranged between 3450 and 2935 cm^{-1}, which correspond to the O–H and C–H stretching vibrations respectively [41, 42]. N-CH_3 band was represented at 2851 cm^{-1} which indicated the presence of TOA solvent [43]. On the middle energy range, decrease or disappearance in the intensity of OH band at 1633 cm^{-1} and high sharp intense band at 1730 cm^{-1} belongs to binding of Zr^{4+} and Y^{3+} to OH− and COO− groups. The band with wavenumber 1360 cm^{-1} ascribed to COO– band of acrylic acid in the composite before and after loading nearly with no change. In the lower energy region, three groups of bands showed an increase in band intensity at 1160 cm^{-1} which could be credited to the confederation between the M–O and CN stretching vibrations of TOA [44]. However, the peak observed at 1025 cm^{-1} was owing to rocking CH_3 and M–O stretching. Deformation or decrease in the intensity of COO– groups bands observed at 620 cm^{-1} were attributed to metal ions interactions with the carboxylic groups of the synthesized resin, respectively.

3.1.5 Thermal Analysis Results

As the IR spectral data indicated the existence of functional groups, thermal analyses (TGA) were done to predict the performance and the chemical degradation characteristics of the synthetic resin and to measure its endothermic and exothermic phase transitions. The thermal stability and phase transitions of the AA-CMC-TOA/rGO sorbent were depicted in Fig. 5. The TGA curve showed three mass loss stages with an overall decrease in the mass of the adsorbent of 95.03%, indicating its low thermal stability. This was attributed to the high content of organic constituents in the matrix of the adsorbent. The first stage, which ran from 46 to 168 degrees Celsius, resulted in a relatively low loss of resin mass of about 3.7% due to the elimination of the aqueous content (water of hydration) as well as the flammable TOA content. Therefore this stage was characterized by an exothermic peak at 154.5 °C which was believed to be caused by the partially separation and evaporation of the solvent content in the resin structure, which was considered to be the initial stage of the decomposition of the compound. Secondly, a significant decrease in the mass of the synthetic resin by 77.7% as a result of the temperature increase, which ranged from 168 to 457 °C, was attributed to the elimination of

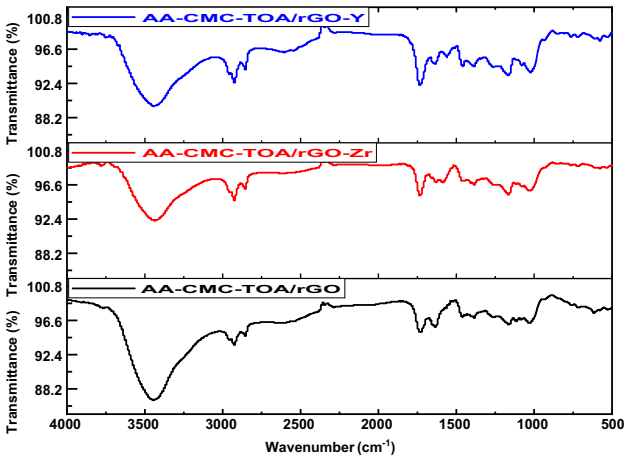

Fig. 4 FTIR-spectra of the AA-CMC-TOA/rGO sorbent, AA-CMC-TOA/rGO-Zr, and AA-CMC-TOA/rGO-Y

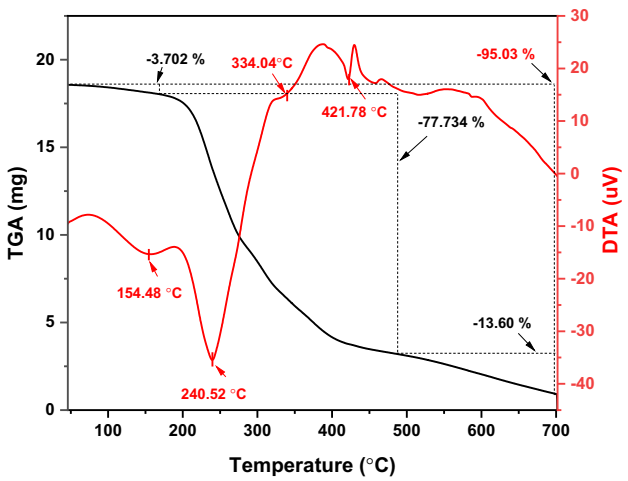

Fig. 5 DTA-TGA chart of the AA-CMC-TOA/rGO sorbent

residual TOA by combustion, and the elimination of water of crystallization, and the conversion of carboxyl groups to carbon dioxide as a result of combustion [29, 45]. As a result of this combustion, a noticeable change in the DTA curve was accompanied, resulting in a three exothermic peaks as shown in Fig. 5. This was believed to be the result of the combustion of different organic contents (CMC, AA, and rGO) causing the formation of different exothermic curves. In the third stage, the TGA curve was indicated with a mass loss of about 13.6% in the 457–700 temperature range, which could be attributed to the combustion of the remained hydrocarbon content of the composite leading to complete removal of the residual organic content and obtaining ash [46]. According to the high thermal stability of rGO with a weight loss of only less than 11% at 800 °C, higher temperatures from 500 to 700 °C resulted in a solid residue of up to 5% of the original resin weight as a result of the non-combustibility of the rGO content [47].

3.1.6 BET Analysis Results

In general, surface area and electronic structure of the composite has an important role in the adsorption process. The BET-surface area, total pore volume, mean pore diameter, and the monolayer adsorbed volume (V_m) of AA-CMC-TOA/rGO porous sorbent were determined from the corresponding N_2 adsorption–desorption isotherm which were found to be 9.7695 $m^2\ g^{-1}$, 0.035 $cm^3\ g^{-1}$, 14.118 nm, 1.65 nm, and 2.245 (cm^3(STP)g^{-1}) respectively. The relatively high surface area characterizing the composite can lead to a suitable capacity for adsorption of Zr^{4+} and Y^{3+} ions. Figure 6a identified the isotherm of composite as a type (I) isotherm according to BET classification and with a type H1 hysteresis loop according to IUPAC classification [48, 49]. The type H1 hysteresis loop characteristics of the microporous material with slit-shape pores or wedge-shaped pores. At low pressures, monolayer formation is beginning whereas at medium pressure, multilayer formation occurs. Figure 6b displayed a narrow pore size distribution of the synthesized sorbent ranging from 3.5 to 10.4 nm.

3.2 Optimization of Adsorption Parameters

3.2.1 Effect of pH

As a result of the direct influence of pH values on the protonation of active sites on the sorbent surface as well as the metal ions species, the effect of pH values on adsorption processes was well investigated [29]. The pH impact was studied using two dissimilar pH ranges of sulfate solutions of Zr^{4+} and Y^{3+} ions separately. The zirconium solution range was from 1.0 to 2.3 and the yttrium solution range was from 1.0 to 5.0. This difference in the pH values was attributed to the different behavior of the two elements when changing the pH values. As illustrated in MEDUSA software shown in Fig. 7c, d, a clear appearance of zirconium oxide precipitate ZrO_2 was observed at the pH of 2.3, this prompted us to study its effect during this narrow range (from 1.0 to 2.3). On the other hand, the beginning appearance of yttrium hydroxide oxide precipitate $Y(OH)_3$ at the

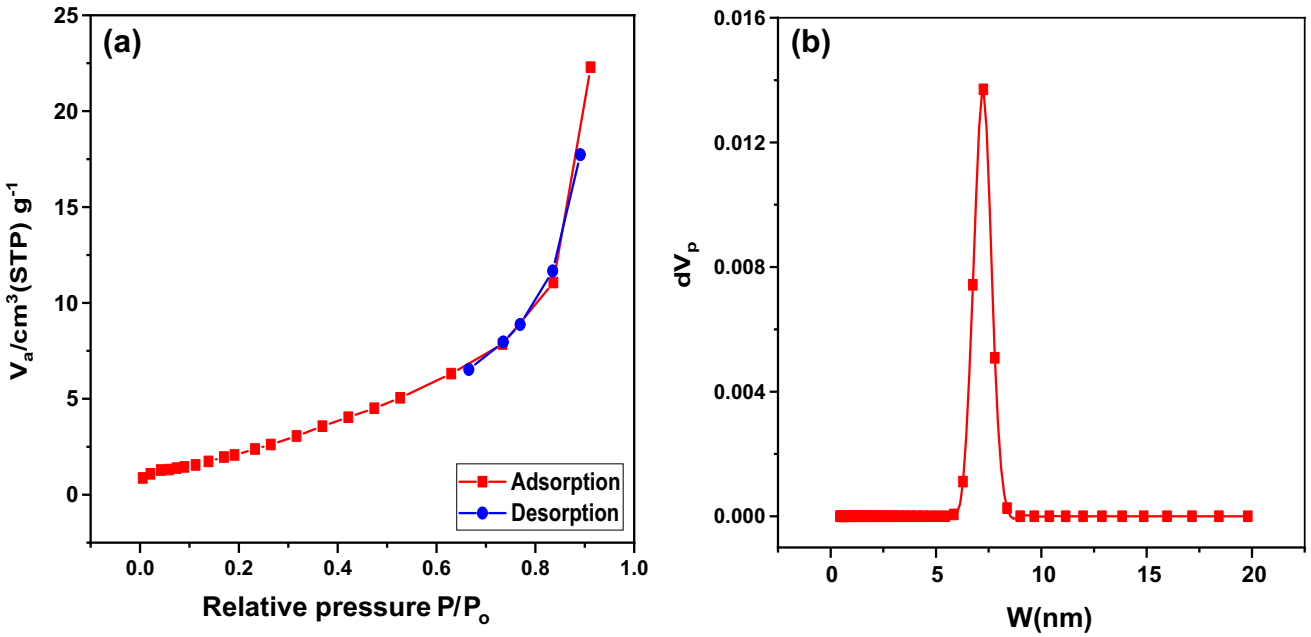

Fig. 6 **a** BET isotherm of the AA-CMC-TOA/rGO sorbent **b** the pore size distribution

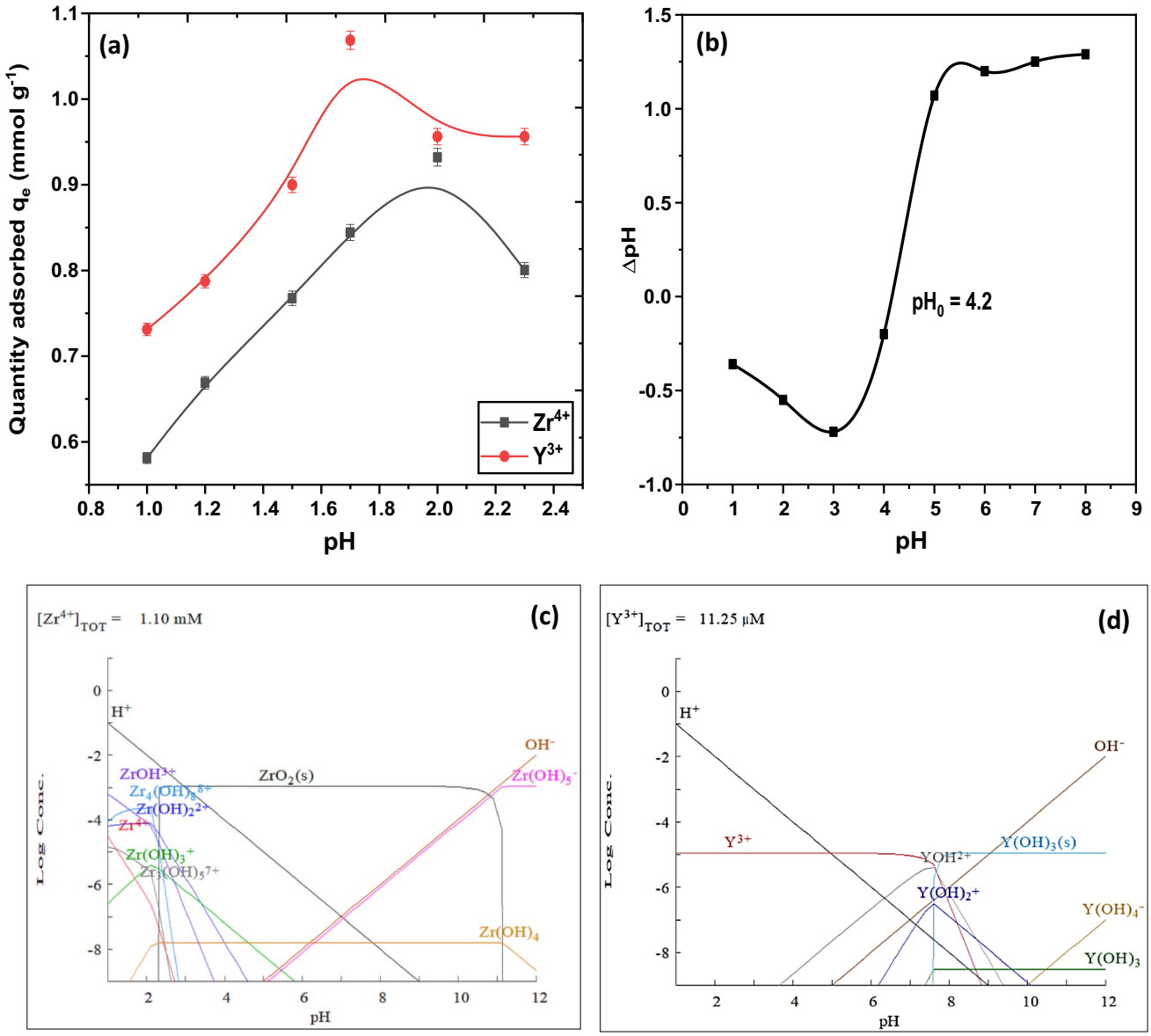

Fig. 7 **a** Effect of pH on the adsorption of Zr^{4+} and Y^{3+} on AA-CMC-TOA/rGO sorbent, **b** determination of pHpzc using pH drift method, **c** speciation of zirconium, and **d** speciation of yttrium at different pH and room temperature

pH of 7.6 prompted us to study the effect of pH on a larger scale (from 1.0 to 5). To scrutinize the chemical formulas of zirconium and yttrium species in the feed solutions, a simulation has been performed using MEDUSA software Fig. 7c. At the studied pH ranges, the predicted species of the two metals were positively charged ions namely; YOH^{2+} and Y^{3+} for yttrium and $Zr(OH)^{3+}$, $Zr_4(OH)_8{}^{8+}$, $Zr(OH)_2{}^{2+}$, Zr^{4+}, $Zr(OH)_3{}^{+}$, and $Zr_3(OH)_5{}^{7+}$ for zirconium. The other constant conditions used in the adsorption parameter were shown in Table 1. Figure 7a displayed sharp increases in the uptake of both zirconium and yttrium ions ranging from 0.58 to 0.93 mmol g^{-1} and from 0.73 to 1.07 mmol g^{-1} by varying the pH of Zr and Y solutions from 1.0 to 4.0 and from 1.0 to 2.0 respectively. So, the pHs of 2.0 and 4.0 were considered the preferable pH values of Zr and Y solutions respectively, and would be applied in the subsequent factors. The decrease in adsorption efficiency of both Zr^{4+} and Y^{3+} ions accompanied by the increase of the pH was attributed to the lower absorption reported in acidic conditions and could be explained by partial protonation of the active sites and increasing the competition between H^+ and Zr^{4+} or Y^{3+} ions for adsorption sites on the resin.

The point of zero charge (pHpzc), at the charge in the adsorbent surface was zero, was determined through a series of experiments with pH changes. The pH of NaCl solutions (0.01 mol L^{-1}) was adjusted using dilute solutions of HCl

and NaOH and ranged from 1 to 8. These initial pH values were taken as pH_i. A specified weight of the absorbent was added to each solution and the final pH (pH_f) was measured after 10 h under stirring at 150 rpm. The chemical and electronic properties of the functional groups localized on the sorbent surface controlled the pHpzc ($pH_i - pH_f = 0$) [50]. From Fig. 7b, the pH pzc of the studied sorbent was 4.2 which mean a positively charged surface below this value. This mean repulsion forces between zirconium and yttrium positive ions and the positively charged surface prevented the interaction between zirconium and yttrium cations and the active sites through weak van der Waal forces (physisorption), which gave evidence of the possibility of chemisorption interaction. This was discussed in detail through the adsorption kinetics outcomes of this study.

3.2.2 Influence of Time

To study and understand the kinetics of the adsorption processes, it was necessary to follow the adsorption of Zr^{4+} and Y^{3+} ions as a function of time.To determine the contact time of the adsorbent-adsorbate interaction at which equilibrium has occurred and maximum uptake has been achieved of Zr^{4+} and Y^{3+} ions, periods from 5 to 120 min were studied using constant conditions as illustrated in Table 1. At ambient temperature, aqueous solution portions with a volume of 10 mL containing 1.097 and 1.125 mmol L^{-1} of Zr^{4+} and Y^{3+} ions each separately and having a pH of 2.0 and 4.0, respectively, were mixed with 20 mg of solid resin using different contact times. Figure 8 showed that the maximum uptakes (sorbed amount) for the Zr^{4+} and Y^{3+} ions 0.987 and 1.012 mmol g^{-1}were achieved within the first 45 min respectively. The high adsorption efficiencies of both metal

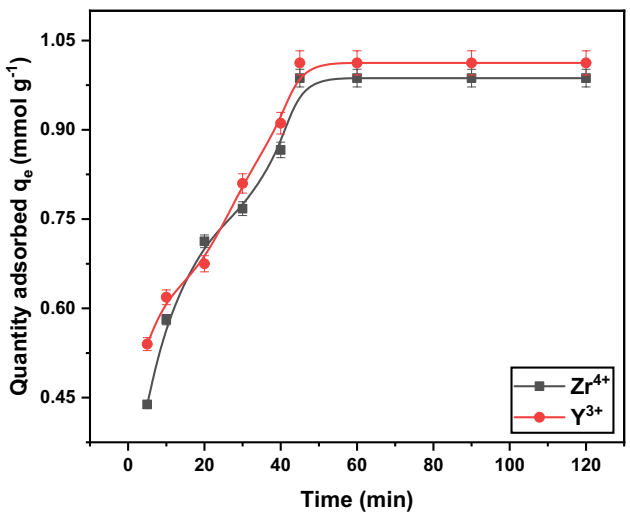

Fig. 8 Effect of time on the adsorption of Zr^{4+} and Y^{3+} on AA-CMC-TOA/rGO sorbent

ions were attributed to the high concentrations of active sites that could be obtained for adsorption at the beginning of the adsorption reactions of both elements. Over time, adsorption rates have been significantly controlled as a result of the occupancy of its active sites and the strict hindrance that belated the rate of arrival of ions to unoccupied active sites.

3.2.3 Sorbent Dose Influence

The purpose of studying sorbent dose factor was to determine the best amount of AA-CMC-TOA/rGO resin capable of adsorbing as much Zr^{4+} and Y^{3+} ions as possible. Using other stationary conditions, namely 10 mL of an aqueous solution containing 1.1 and 1.13 mmol L^{-1} with a pH of 2.0 and 4.0 of Zr^{4+} and Y^{3+} ions, respectively, 45 min stirring time, and under 298 K, various amounts of AA-CMC-TOA/rGO sorbent alternating from 10 to 50 mg have been checked to investigate the effect of sorbent dosage. It was agreed that the greater the weight of the sorbent with fixed concentrations of metal ions, the higher the adsorption efficiency. The adsorption efficiency was inversely proportional with the loading capacity of the sorbent. This could be explained by the fact that when a small amount of the synthesized resin was used, it was rapidly saturated with metal ions and was accompanied by poor adsorption efficiency. Whereas when large amounts of resin were used with the same solution, the ion adsorption efficiency increased dramatically, and complete saturation of the resin with the initial ions may not occur due to the abundance of the sorbent material at the expense of the content of ions existing in the solution. From the results shown in Fig. 9a, significant decreases in the sorbed amounts of Zr and Y ions were detected when the resin mass was increased from 10 to 50 g. These sorbed amounts have been reduced from 0.99 to 0.22 mmol L^{-1} and from 1.07 to 0.23 mmol L for zirconium and yttrium, respectively, as a logical consequence of the increased availability of AA-CMC-TOA/rGO active sites resulting from the increased sorbent dose.

3.2.4 Influence of Metal Ions Concentrations and Adsorption Temperature

Elemental concentration was a strong driving force in overcoming all resistances of metal ions to mass transfer between different phases. The metal ion concentration affected the performance of the adsorption reaction in the range of 0.27 to 2.19 mmol L^{-1} and from 0.28 to 2.5 mmol L^{-1} for Zr^{4+} and Y^{3+} respectively. The sorbed amount augmented with the growth in concentration owing to the increase in the zirconium and yttrium ions contents at the composite surface and consequently increased driving force movement [51]. Fixed conditions of 10 mg sorbent, 10 mL sulfate solution, 45 min adsorption time, pH 2.0 and 4.0 were used for

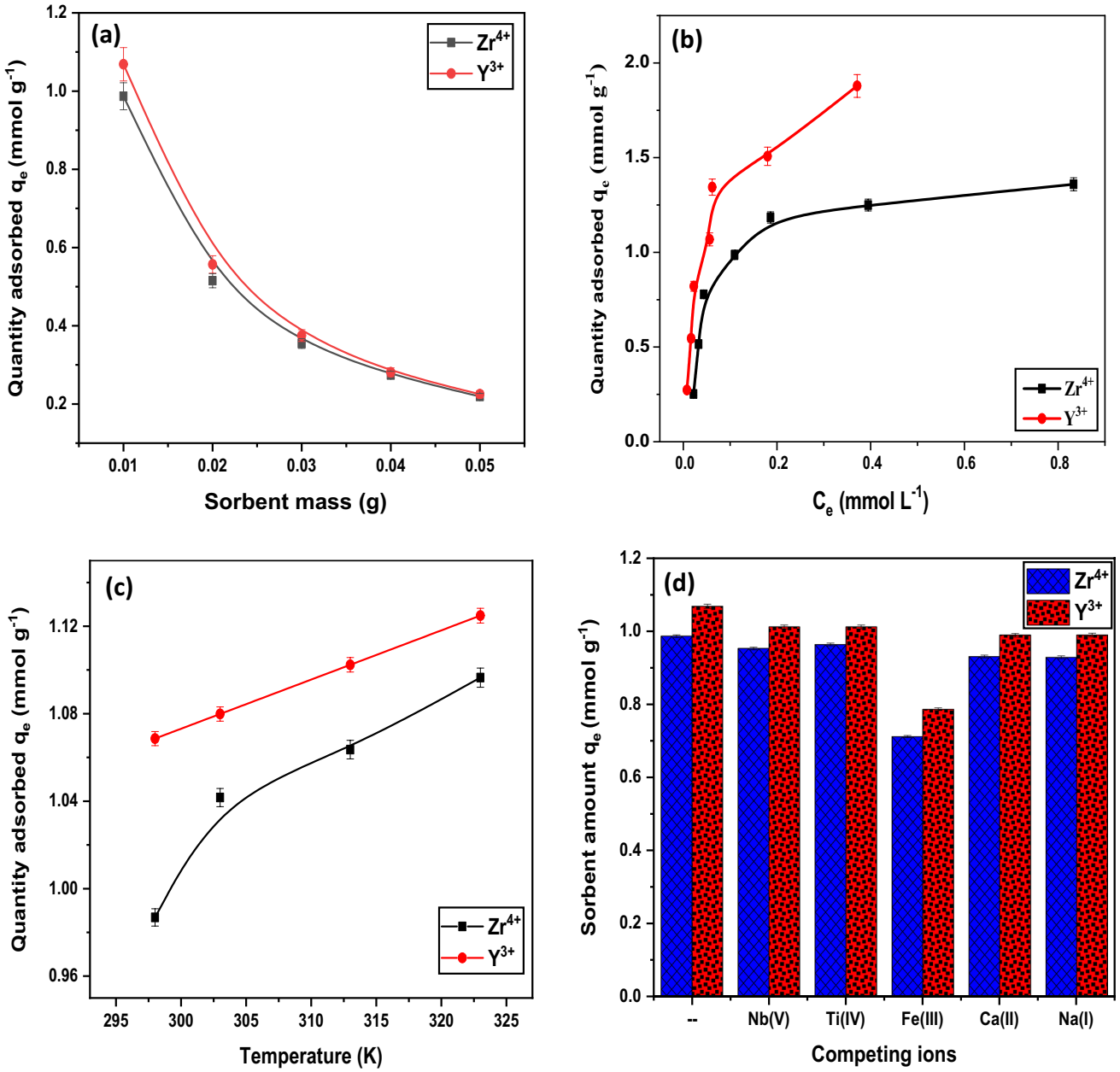

Fig. 9 **a** Effect of the sorbent dose, **b** the initial concentration, **c** the adsorption temperature, and **d** the competing ions on the adsorption of Zr^{4+} and Y^{3+} on AA-CMC-TOA/rGO sorbent

Zr^{4+} and Y^{3+} ions in a temperature range (298 to 323 K) respectively.

From Fig. 9b, by increasing the metal ion concentrations, the sorbed amounts of both Zr^{4+} and Y^{3+} ions on AA-CMC-TOA/rGO adsorbent were augmented and reached 0.99 and 1.07 mmol g^{-1} using 1.10 and 1.13 mmol L^{-1} initial concentrations of Zr^{4+} and Y^{3+} ions respectively. Using 2.19 and 2.25 mmol L^{-1} initial concentrations of Zr^{4+} and Y^{3+} ions has a positive effect and enhanced the sorbed amounts to 1.95 and 2.05 mmol g^{-1} respectively. In general, the improvements in the adsorption of both metal ions by increasing their initial concentrations were attributed to increasing the potentiality of binding with the permitted active sites localized on the composite. As the initial concentration of Zr^{4+} and Y^{3+} ions increased, the occupancy of adsorption zones on the surface of the manufactured material increased causing a reduction in the sorbed amount of both metal ions. As shown in Fig. 9b, a sharp increase in the uptake of zirconium than yttrium was observed indicating a variance in the adsorption of the two metal ions. This could be attributed to the appearance of polyvalent cations of zirconium metal (7 types), while

yttrium has only two types of positive ions with lower valence as shown in Fig. 7c, d.

In contrast to yttrium ions, this extreme diversity of zirconium ions carrying + 8, + 7, and + 4 charges resulted in a strong attraction with the negatively charged existing on the composite active sites. On the other hand, Zr^{+4} ionic radius was 0.080 nm while Y^{3+} in eightfold coordination was estimated to be 0.1011 nm measured by using the lattice parameters and the empirical equations to predict the lattice parameters of the fluorite-type solid solutions. This difference in atomic radius of both ions could play a significant role in the attendance of each metal ion toward the active group of the synthesized adsorbent [52]. In addition, the charge density of zirconium ions was 224 C mm^{-3}, which is higher than the charge density of yttrium ion 110 C mm^{-3} [53]. This indicated the preferability of Zr^{+4} ions over Y^{3+} ions to interact with active sites of the AA-CMC-TOA/rGO composite.

The effect of reaction temperature was studied from 298 to 323 K using constant factors namely 10 mg adsorbent, 10 mL aqueous solution of 1.10 and 1.13 mmol L^{-1} metal ion concentrations, 45 min adsorption time, and pH 2.0 and 4.0 for Zr^{4+} and Y^{3+} ions respectively. From the temperature effect curves (Fig. 9), it was clearly obvious that the increase in the adsorption temperature was a positive factor as the absorption efficiency of the ions of both elements increased. Experimentally, the adsorption of zirconium and yttrium ions increased from 0.99 and 1.07 mmol g^{-1} at room temperature to 1.10 and 1.13 mmol g^{-1} at 323 K, respectively. This could be elucidated by the fact that the high temperature increased the kinetics of the reactants, provided the required activation energy for the molecules of the reactant, and thus increased the chemical adsorption processes.

3.2.5 Influence of Competing Ions

The effect of the presence of competing elements on the adsorption effectiveness of Zr^{4+} and Y^{3+} ions was studied to determine the ability of the resin to extract the ions of the two target elements in the attendance of the other ions. These treatments were carried out using the best adsorption results that were previously mentioned during this study namely, 10 mg of the AA-CMC-TOA/rGO sorbent, stirring for 45 min at ambient temperature 10 mL of acidic solution of pH 2.0 and 4.0 containing 1.10 or 1.13 mmol L^{-1} of Zr^{4+} or Y^{3+} ions respectively. Specific concentrations of different metal ions namely Nb^{5+}, Ti^{4+}, Fe^{3+}, Ca^{2+}, and Na^{+} were added separately with equi-concentration of Zr^{4+} or Y^{3+} ions without an increase in the volume of the acidic solution (10 mL). Each solution used during this factor contained an equal concentration of the competing and the studied element. The competing ions results on the AA-CMC-TOA/rGO sorbent were shown in Fig. 9d. All elements except iron have a weak impact on the sorbed amounts of both Zr^{4+} and Y^{3+} ions on the sorbed surface. It has also been observed that the effect of competition was slightly higher in the case of zirconium compared to yttrium. The rates of reduction in the sorbed amounts of Zr^{4+} and Y^{3+} ions in the presence of competing iron ions were 27.8 and 26.3% respectively. From the MEDUSA curves for zirconium and yttrium ions as shown in Fig. 7c, d, it was evident that most of the yttrium and zirconium ions were present as trivalent ions namely Y^{3+} and $Zr(OH)^{3+}$ respectively, which might explain the strong contrast between them and trivalent iron.

3.2.6 Influence of Binary System

After completing the study of various factors affecting the adsorption processes of zirconium and yttrium ions, as well as the effect of adding other competing ions, the effect of the presence of both elements side by side in a binary system was investigated. The adsorption efficiencies of zirconium and yttrium ions as well as the detection of their separation factors were determined from binary system studies. At the outset, it should be noted that the best suitable conditions were used to separate the two elements, which were similar in most situations except for the pH of the acidic medium, where all the experiments were conducted at pH 2.0 in agreement with the zirconium adsorption results. As previously decided, the sorption tests were carried out at pH 2.0 to avoid precipitation of the zirconium content when the pH was raised above 2.0 as shown in Fig. 7. The other constant factors were 10 mg of the AA-CMC-TOA/rGO sorbent, 10 mL of acidic solution both 1.10 and 1.13 mmol L^{-1} of Zr^{4+} and Y^{3+} ions respectively, stirring for 45 min at ambient temperature. In Table 2, the sorbed amounts of Zr^{4+} and Y^{3+} ions and their distribution coefficient (K_d) were determined in the individual and binary systems to understand the mobility of their ions between the two media and their distribution between the composite and the aqueous solution.

Table 2 Individual and binary systems results

	Individual system		Binary system			
	Quantity adsorbed, mmol g^{-1}	K_d	Quantity adsorbed, mmol g^{-1}	K_d	$S_{Zr/Y}$	$S_{Y/Zr}$
Zr^{4+}	0.99	9	0.89	4.26		
Y^{3+}	1.07	19	0.78	2.23	1.915	0.522

In addition, separation factors ($S_{Zr/Y}$, $S_{Y/Zr}$) were also calculated for the binary system, which was the distribution coefficient of metal ion divided by other and was a measure of the system's ability to separate two solutes. From the mentioned table, the absorbed amount of yttrium ions decreased by about 27.4% in the binary system, while the absorbed amount of zirconium ions decreased by about 10%. This decrease was accompanied by an expected decrease in K_d values (from 9 to 4.26 and from 19 to 2.23 for Zr^{4+} and Y^{3+} ions respectively). It was believed that the apparent reduction in the adsorption uptakes of both metals was due to the competitiveness between the species of the two metal ions for the active sites located on the surface of the composite. On the other hand, the relatively lower adsorption of yttrium ions compared to zirconium ions could be attributed to the use of appropriate pH of zirconium, which was not considered an optimal choice for yttrium. Moreover, the presence of different zirconium ions with a high positive charge compared to yttrium created competition between the ions of the two elements in favor of the zirconium ions. As discussed in effect of concentrations of metal ions, the atomic radius of both metal ions and their charge density played an essential role in the preference of Zr over Y ion. This led to a tendency for zirconium ions to adsorb preferentially over yttrium ions as indicated by their separation factor values.

3.3 Adsorption Isotherm, Kinetic, and Thermodynamic Results

3.3.1 Adsorption Isotherm

Four models were used to study the adsorption of Zr^{4+} and Y^{3+} on AA-CMC-TOA/rGO adsorbent namely, Langmuir, Freundlich, Redlich–Peterson and Dubinin–Radushkevich models to determine the optimal model that explained the reaction mechanism. The applied model's fitting curves at 298 K were collected and drawn in Fig. 10 and their corresponding evaluated parameters were listed in Table 3. The R^2 values and the error functions χ^2 were considered the tools for selecting the best fitted models. The highest R^2 and lowest χ^2 values revealed that the sorption mechanism was regulated by the Langmuir isotherm for both metal ions upon the AA-CMC-TOA/rGO surface. These results were taken as the second evidence to confirm the proposal of the chemisorption mechanism of both Zr^{4+} and Y^{3+} on the synthesized resin. B values for the Redlich–Peterson model were 0.966 and 0.949 close to unity for Zr^{4+} and Y^{3+}, respectively confirming the fitting of the Langmuir mechanism for the sorption reaction as well as implying chemisorption nature [54]. Zirconium and yttrium sorption onto the AA-CMC-TOA/rGO sorbent has monolayer adsorption uptakes of 1.47 and 1.99 mmol g^{-1} at 298 K respectively. The D-R isotherm model was characterized by high R^2

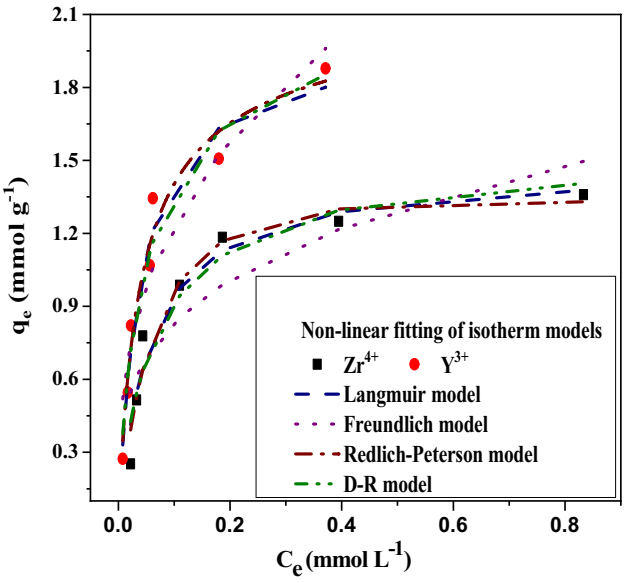

Fig. 10 Adsorption isotherm modeling of Zr^{4+} and Y^{3+} on AA-CMC-TOA/rGO sorbent

Table 3 Adsorption isotherm parameters of Zr^{4+} And Y^{3+} onto AA-CMC-TOA/rGO composite

Parameters	Adsorption isotherm models	
	Zr^{4+}	Y^{3+}
Langmuir model		
q_m (mmol g^{-1})	1.470	1.993
K_L	17.877	25.182
R^2	0.941	0.959
χ^2	0.0099	0.012
Freundlich model		
n	3.614	2.903
K (mmol $n^{-1}g^{-1}.L^{-n}$)	1.573	2.757
R^2	0.778	0.889
χ^2	0.0371	0.035
Redlich–Peterson model		
K_{RP}	22.34	55.799
a_{RP}	15.85	26.505
B	0.966	0.949
R^2	0.936	0.9507
χ^2	0.011	0.0156
Dubinin–Radushkevich model		
q_{mDR} (mmol g^{-1})	1.482	2.0997
β_{DR} (mmol^2 kJ^{-2})	0.08434×10^{-8}	0.07302×10^{-8}
E (kJ mol^{-1})	24.348	26.168
R^2	0.9241	0.953
χ^2	0.0121	0.0148

The highest R^2 and lowest χ^2 are underlined

values and the adsorption energies E calculated were 24.348 and 26.168 kJ mol^{-1} more than 8 kJ mol^{-1}which proved its adsorption chemically [55].

3.3.2 Adsorption Kinetic

Figure 11 depicted the non-linear regression fitting plots of pseudo-1st-order, pseudo-2nd-order, Elvoich, and pseudo-nth-order models and Table 4 listed the kinetic parameters for the applied kinetic modeling. With respect to the calculated q_t of pseudo-first-order and pseudo-second-order were closer to the experimental q_t of Zr^{4+} and Y^{3+} uptake. Applying error functions R^2 and χ^2 for selecting the best-fit model, pseudo 2nd order was the highest one for R^2 while pseudo-nth-order was the best-fit model using χ^2 error function for the lowest value. This implied that the sorption reaction was performed via a chemical reaction mechanism. So, this aimed to point out the low performance of R^2 and its inappropriateness for the non-linear regression model [56]. Thus the accurate order of the sorption reaction was 1.744 for Zr^{4+} and 2.177 for Y^{3+} ions. From the results shown, it was proved that the adsorption reaction corresponds to the chemical adsorption mechanism according to the results of isothermal adsorption.

3.3.3 Adsorption Thermodynamic

Using Eq. (13), straight lines of intercept and slope equal to $\Delta S^o/R$ and $\Delta H^o/R$ were gained from the plotting of ln

Table 4 Kinetic models parameters and error functions data for the sorption of Zr^{4+} and Y^{3+} onto AA-CMC-TOA/rGO composite

Parameters	Time transient model	
	Zr^{4+}	Y^{3+}
q_t (mmol g^{-1}) (experiment)	0.99	1.07
Pseudo-first order		
q_t (mmol g^{-1}) (calculated)	0.96	1.03
K_1 (min^{-1})	0.0843	0.0795
R^2	0.863	0.706
χ^2	47.11	108.43
Pseudo-second order		
q_t (mmol g^{-1}) (calculated)	1.08	1.15
K_2 (g mg^{-1} min^{-1})	0.0012	0.0011
R^2	0.938	0.875
χ^2	21.208	46.073
Elovich kinetic model		
α (mmol g^{-1} min^{-1})	0.39	0.44
β (g mg^{-1})	0.0563	0.055
R^2	0.917	0.835
χ^2	28.55	60.567
Pseudo nth order		
n	1.744	2.177
kn (kg^{n-1} g^{1-n} min^{-1})	0.0598	7.887×10^{-8}
R^2	0.888	0.7104
χ^2	0.0044	0.0099

The highest R^2 and lowest χ^2 are underlined

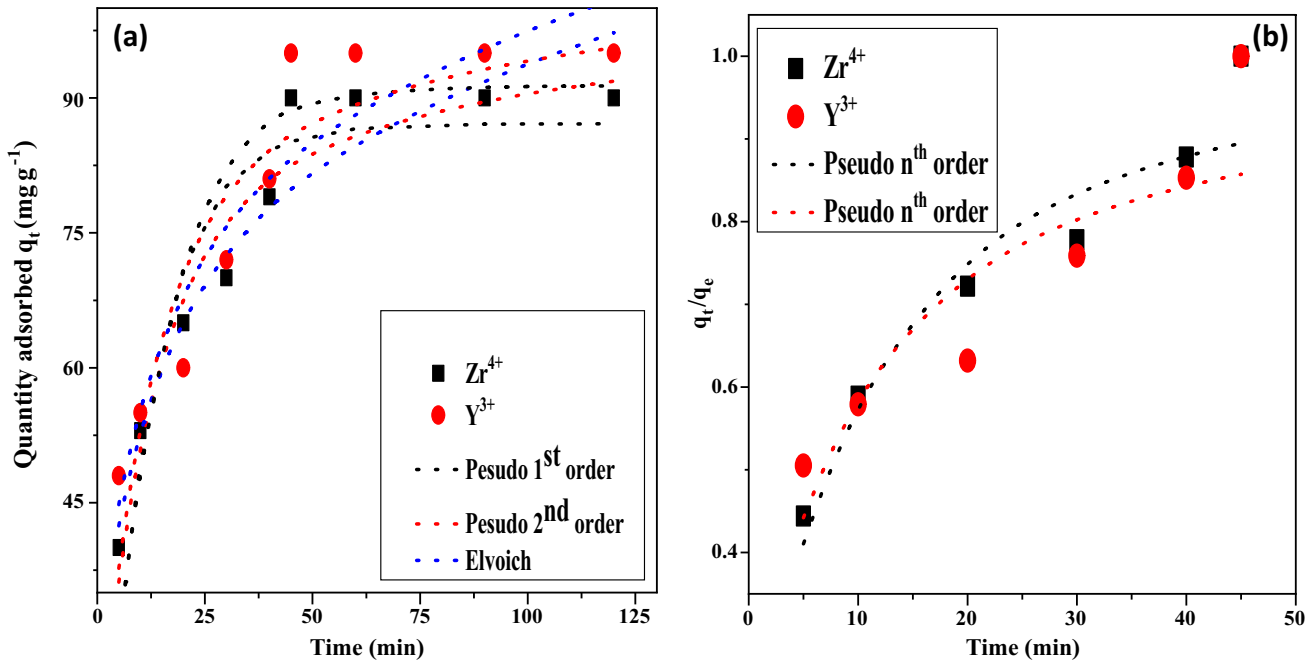

Fig. 11 **a** Pseudo 1st, 2nd, and Elvoich and **b** pseudo nth order Kinetic modeling fitting sorbent of Zr^{4+} and Y^{3+} on AA-CMC-TOA/rGO

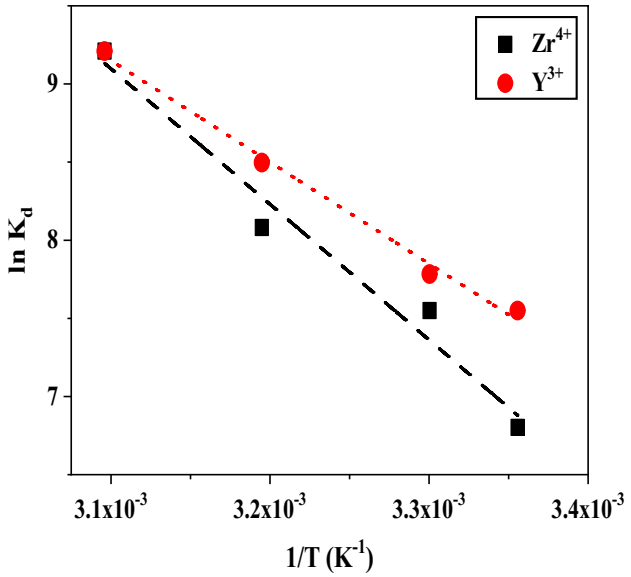

Fig. 12 Thermodynamic curves for Zr^{4+} and Y^{3+} adsorption on AA-CMC-TOA/rGO composite

K vs. 1/T, respectively (see Fig. 12). the thermodynamics parameters ΔS^o and ΔH^o were calculated and stated in Table 5. The positive values of ΔH^o for both elements indicated the endothermic nature of the adsorption reactions of Zr^{4+} and Y^{3+} ions on the functional groups diffused on the surface of the synthesized AA-CMC-TOA/rGO resin, favoring an external energy source, showing a positive effect with increasing temperature. From the results of the ΔS^o values with a positive sign, an increase in the randomness of the system appeared in the adsorption processes for each of the metal ions between the positive ions and the active sites on the surface of the adsorption material. On the other hand, through Eq. (14), $\Delta G°$ was calculated for the adsorption processes of both elements on the surface of the used resin. It was shown from the negative sign of the above coefficient that the adsorption process was feasible, spontaneous, and directly affected by a high degree of interaction, which in turn positively affects the ability of element ions to easily reach the active sites and the functional groups scattered on the resin surface. Finally, by calculating the values of $T\Delta S°$, which clearly lower than the values of $\Delta H°$ as the temperatures of the adsorption processes changed, it turns out that entropic changes dominated the adsorption [34, 57].

3.4 Adsorption Mechanism

Initially, before the irradiation process, several reactions occurred between acrylic acid on the one hand and CMC, rGO, and TOA on the other. grafted carboxy methyl cellulose gel (GCMC) and other intermediate compounds were formed as discussed in previous works [22, 34, 58]. The intermediate compounds were shown in Fig. 13. Before the irradiation process, small additions from the MBA crosslinker was added to these intermediate mixture as shown in Fig. 13. As a result of radiation exposure, many of the double bonds present in acrylate compounds (A, B, and C) and MBA were broken, producing relatively large numbers of free radicals, which caused the polymerization and the production of AA-CMC-TOA/rGO sorbent. CMC and PAA served as a spine for the manufactured composite by forming two interlocking chains backed by rGO. Both formed chains contained many functional groups such as carboxylic (–COOH), hydroxyl (–OH), and secondary amine groups (R_2NH), indicating the presence of dense active sites on the surface of the manufactured resin capable of attracting zirconium and yttrium positive ions. An electrostatic attraction between these groups and both metal ions has already been suggested as shown in Fig. 14.

3.5 Desorption and Stability Studies Results

In order to recover Zr^{4+} and Y^{3+} ions from the loaded AA-CMC-TOA/rGO resin, two mineral acids were tested with two different concentrations, namely sulfuric acid and hydrochloric acid. Initially, the effectiveness of using hydrochloric acid in comparison to sulfuric acid was observed using both concentrations. From the outcomes displayed in Fig. 15a, it can be seen that the recovery efficiencies of both metal ions were enhanced by using 1.0 mol L^{-1} instead of using 0.5 mol L^{-1} for both acids. Desorption efficiencies of 72 and 80% were achieved using 0.5 mol L^{-1} H_2SO_4 while 82 and 90% were attained using 1.0 mol L^{-1} H_2SO_4 for the Zr^{4+} and Y^{3+} ions, respectively. On the other hand, increasing the concentrations of HCl from 0.5 to 1.0 mol L^{-1} changed the recovery efficiencies from 85 and 88% to 98 and 99% for Zr^{4+} and Y^{3+} ions, respectively. Therefore, 1.0 mol L^{-1} HCl was considered the most appropriate eluent under other constant namely 60 min stirring time, 1/5 solid to aqueous ratio and at room temperature. The stability of the compound was examined using several soaking solutions with a concentration of

Table 5 Thermodynamic parameters for Zr^{4+} and Y^{3+} sorption onto AA-CMC-TOA/rGO composite

Composite	Δ H kJ mol^{-1}	ΔS J mol^{-1} K^{-1}	ΔG kJ mol^{-1}			
			298 K	303 K	313 K	323 K
AA-CMC-TOA/rGO	72.11	298.68	− 16.23	− 17.73	− 20.71	− 23.70

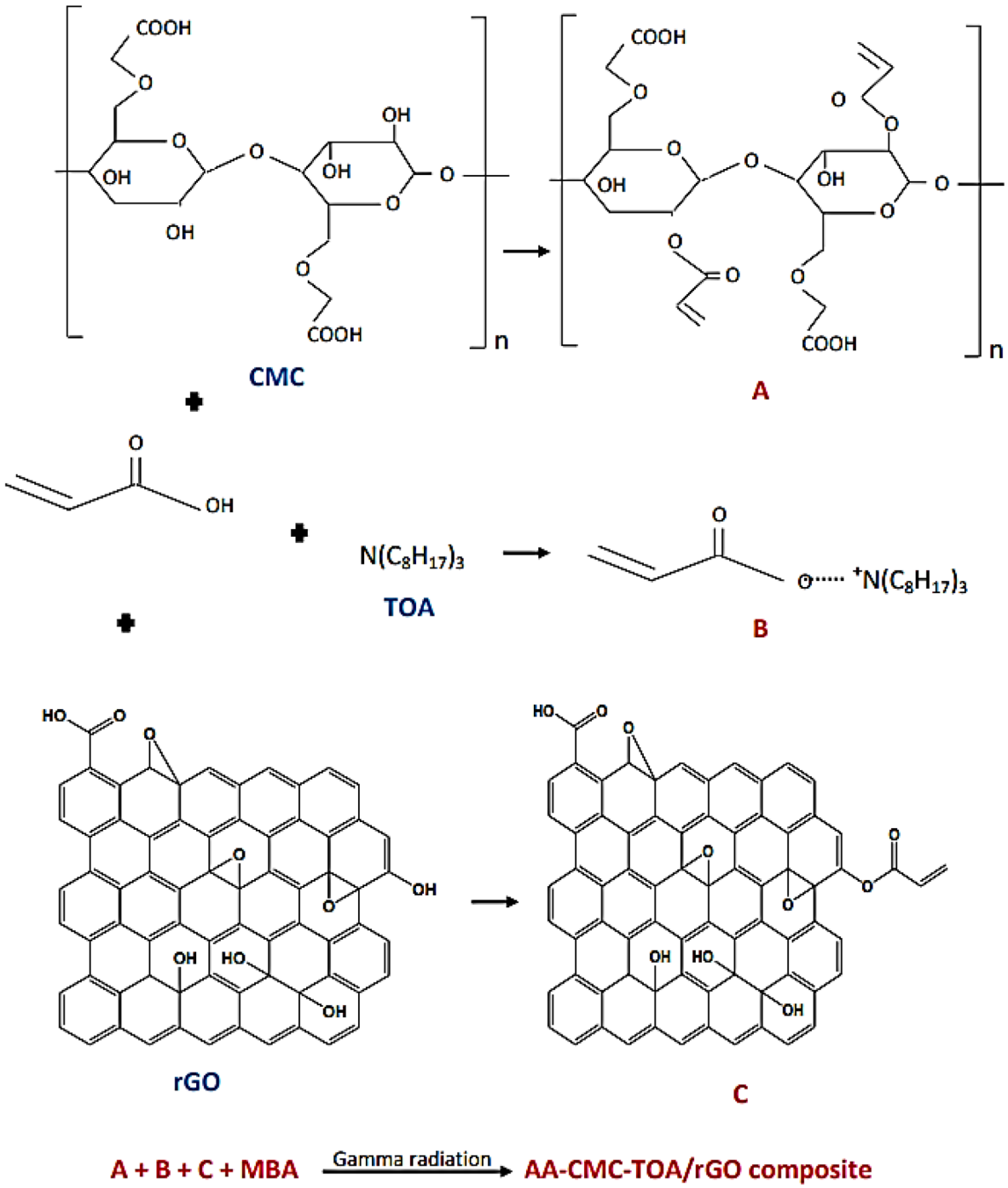

Fig. 13 A suggested diagram for the preparation and the polymerization of AA-CMC-TOA/rGO sorbent

1.0 mol L^{-1}, namely HCl, H_2SO_4, HNO_3 and NaOH. After 24 h soaking time, the remaining composites were filtered, dried at 333 K for 6 h, weighed, and finally compared to their original weights. Figure 15b showed the remaining mass percentages of the different absorbents after soaking in the different solutions. Sodium hydroxide has a serious effect on the shape of the resin by changing its color from black to white and swelling its particles. These influences could alter the physical and chemical properties of the studied composite. All acids didn't have any morphological changes and degradation effects on the sorbent. From Fig. 15b, the sorbent decomposition in sulfuric and hydrochloric acids may be neglected according to the rare mass losses of the sorbent. Soaking in nitric acid has a mild decomposition effect due to a decrease in the remaining mass percentage by 89%. Therefore, sulfuric and hydrochloric acids were the most suitable soaking solutions for applying adsorption and desorption processes.

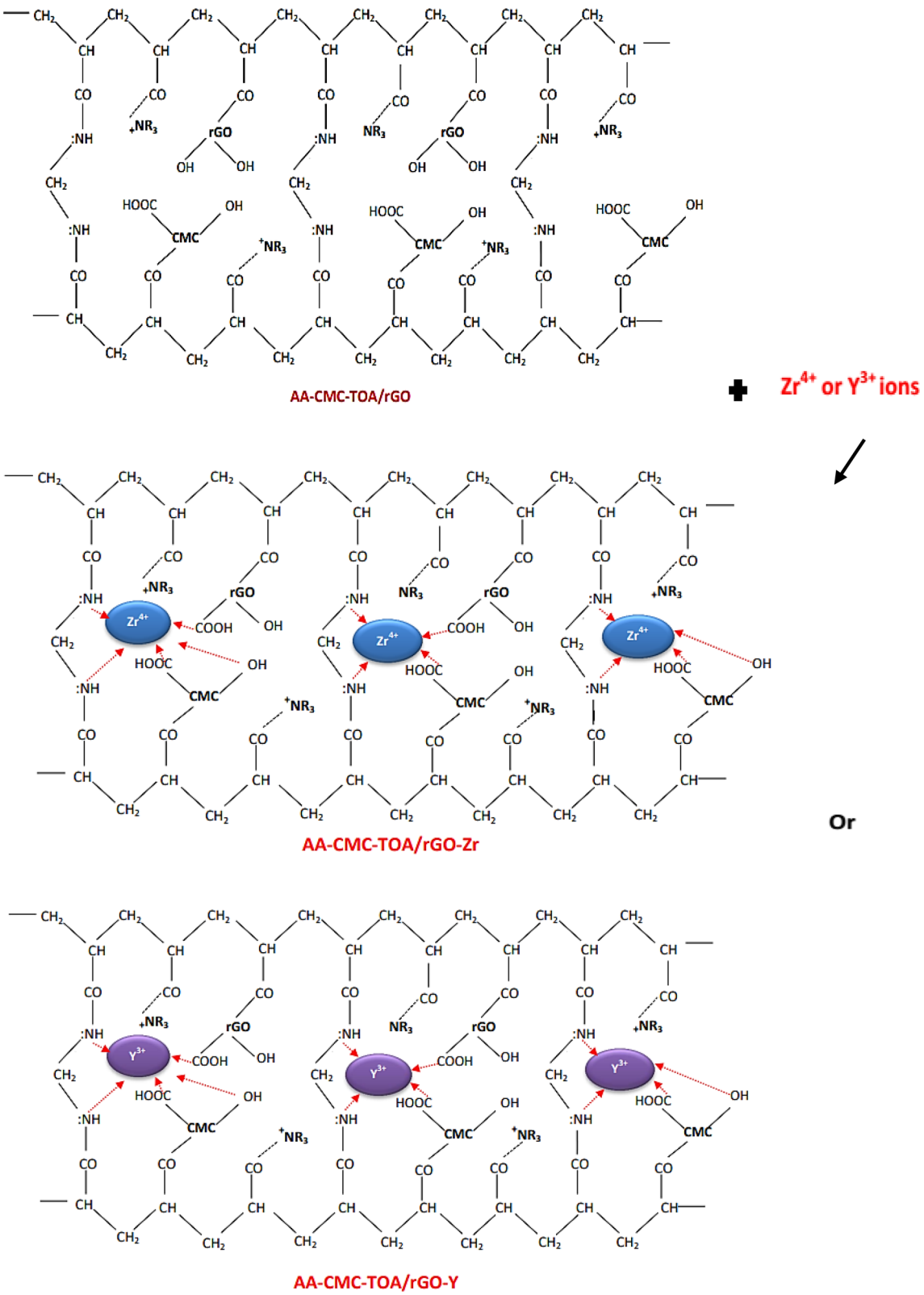

Fig. 14 The prediction mechanism for the adsorption of Zr^{4+} and Y^{3+} ions upon AA-CMC-TOA/rGO sorbent

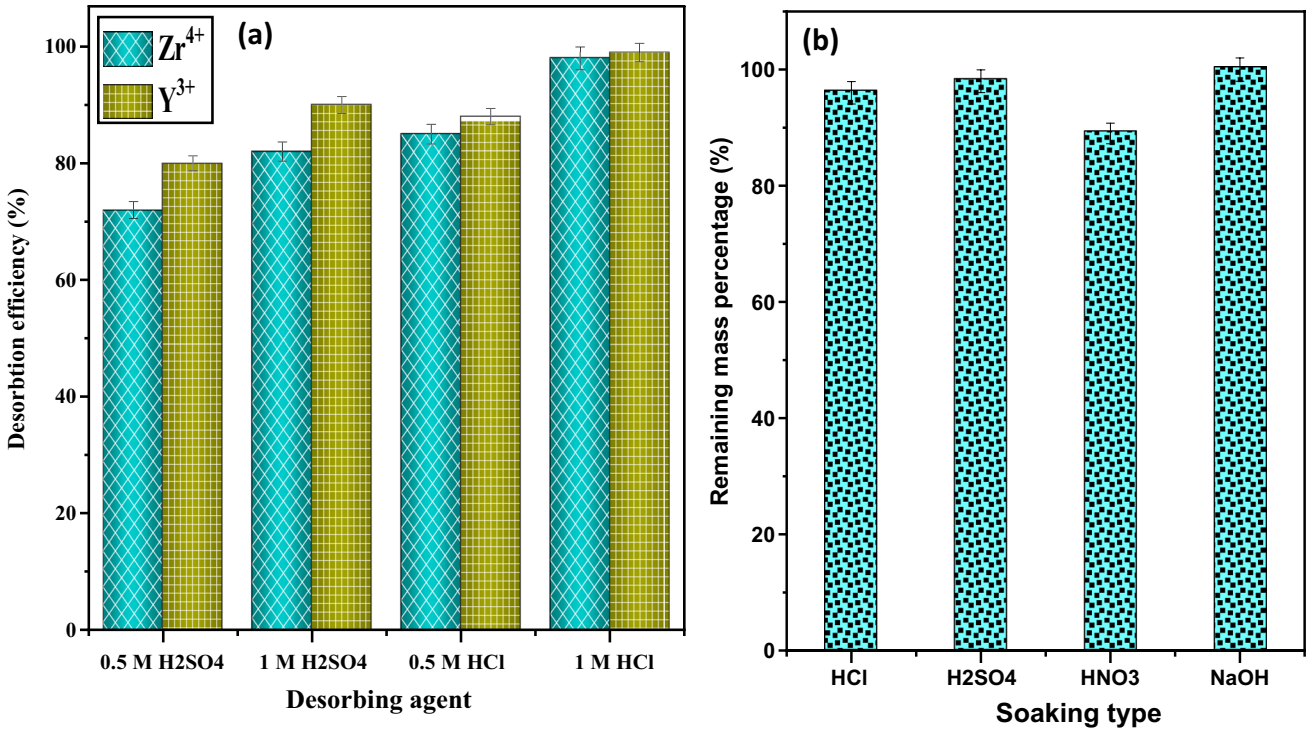

Fig. 15 **a** Desorption efficiencies of Zr^{4+} and Y^{3+} ions and **b** remaining mass percentages of AA-CMC-TOA/rGO composite after soaking in different solutions

3.6 Real Application Results

The technique of using the AA-CMC-TOA/rGO composite as adsorbents for zirconium and yttrium ions was applied from an effluent solution received from NMA laboratories and containing several competing ions beside the two desired metal ions. As shown in Table 6, there were respectable contents of both metal ions required to be practicably withdrawn using the optimum regulatory parameters affecting the adsorption, which were proven during this study such as the raffinate pH of 2.0, 100 mg of the AA-CMC-TOA/rGO sorbent, 100 mL of acidic solution, and stirring for 45 min at ambient temperature. As a result of adsorption–desorption processes of Zr and Y ions, 86 and 60% were the recovery efficiencies of both metal ions respectively. The average recovery efficiencies could be attributed to the presence of many other co-elements such as Si, Cl, Ti, V, K and Na. These enormous concentrations of interfering ions (at concentrations several times greater than the desired elements as shown in Fig. 9) decreased and affected the adsorption of the studied resin. As a result of the limited active sites on the surface of the sorbent, as well as the intense competition

Table 6 Distribution of different ions concentrations in the laboratory waste solution before and after the adsorption on the AA-CMC-TOA/rGO sorbent

Parameter	Initial concentration (mg L^{-1})	Final concentration after adsorption (mg L^{-1})	Sorption amount (mg g^{-1})	Sorption efficiency (%)
V	100	97	3	3
Zr	120	16	104	86.67
Ti	66	54	12	18.18
Si	200	173	27	13.5
Cl-	750	670	80	10.66
K	640	622	18	2.81
Na	252	239	13	5.158
Y	80	32	48	60

Sorption amount and sorption efficiencies for Zr^{4+} and Y^{3+} ions are underlined

between these enormous concentrations and the low contents of desired elements ions, the decrease in the sorbed amounts of both elements was relatively great surpassing the results obtained from the previously mentioned of the competing ions effect. Therefore, this led to a reduction in the adsorption efficiency of the studied element, which requires more purification work. These efficiencies could be overcome by using either a higher amount of the sorbent or by making another contact between the acidic solution and the sorbent. In general, the sorbent successfully recovered the Zr and Y ions from the waste solution. After the adsorption–desorption processes, a concentrated eluate solution was obtained containing the Zr and Y ions at concentrations of 173 and 120 times the initial concentration of the effluent solution respectively.

In addition, it should be noted that both elements could be easily separated from each other using the oxalic acid precipitation technique [59]. This could be achieved after raising the acidic eluate pH to 2.0 using sodium hydroxide solution (50%), stoichiometric amounts of oxalic solution (12%) were added to the solution until reaching the pH 1.0, and the precipitate was finally washed with diluted oxalic acid solution (1%) and followed with distilled water. The remained effluent solution would be exposed to complete precipitation for the zirconium content using ammonia at pH 9.0 [10]. The ammonium precipitate would be washed several times, dried, and calcined. These results demonstrated the ability of the synthesized AA-CMC-TOA/rGO resin to recover Zr and Y contents from the waste solutions. As shown in Table 7, when the resin adsorption results were compared to previous works, the ability of the composite to successfully recover both components was demonstrated and yielding relatively high recovery efficiencies.

4 Conclusion

Gamma-ray polymerization technology was employed to perform selective synthesis of an AA-CMC-TOA/rGO composite that will serve as an innovative adsorbent for Zr^{4+} and Y^{3+} ions. Using the synthesized composite as a sorbent was investigated, and its tests made on synthetic solutions to ascertain optimal adsorption conditions. Approximately 0.99 and 1.07 mmol L^{-1} as sorbed amounts of Zr and Y ions were accomplished using 1/1000 resin/aqueous ratios (g/mL), pH of 2.0 and 4.0, stirring for 45 min at 298 K, and metal ion concentrations of 1.06 and 1.13 mmol L^{-1} respectively. The complete characterization of the loaded and unloaded AA-CMC-TOA/rGO composite was performed using different suitable techniques, demonstrating the successful occurrence of the polymerization, and confirming the occurrence of the adsorption of the metals ions, as well as explaining the nature of active sites and functional groups localized on the resin surface responsible for the adsorption

Table 7 A comparative study between different adsorbents on their adsorption capacities for Zr^{4+} and Y^{3+} ions

Adsorbent material	Adsorption capacity (mmol g^{-1})		References
	Zr^{4+}	Y^{3+}	
Carbonized Spent Bleaching Earth (CSBE)	–	0.61	[60]
Polyethylenimine (PEI)-scaffolded and functionalized grapheme aerogel (PEI-GO-AG)	–	0.43	[61]
Nano-composite cation exchanger sodium dodecyl sulfate acrylamide Zr(IV) selenite (SDS-AZS)	–	0.24	[62]
3-Amino-5-Hydroxypyrazole Impregnated Bleaching Clay (AHIBC)	–	1.93	[63]
Ion imprinted polymers Y(III)-IIPs	–	0.12	[64]
Pectin-Chitosan	–	0.26	[65]
Sulfadiazine schiff base (SDSB)	–	0.9	[9]
Dowex 50WX8 50	1.89	–	[66]
Amberlite	1.64	–	[66]
Phosphoric acid containing (GMA-DVB)-magnetic resin	0.94	–	[67]
Silica gel bound crown ether SGN18	0.42	–	[68]
Phosphoric acid based ligand functionalized silica gels MPFSG	0.14	–	[69]
BPFSG	0.18	–	[69]
AAPPFSG	0.32	–	[69]
Modified Silica Gel PGMS	0.79	–	[70]
SGMS	0.49	–	[70]
Reduced graphene oxide composite rGO-g-PAA-MA/TOA	0.82	–	[22]
AA-CMC-TOA/rGO sorbent	0.99	1.07	This study

processes of both metal ions. The adsorption consequences were studied using several isothermal and kinetics models. The models explain the adsorption process by grasping the adsorption mechanism. These models proved the chemical nature of the adsorption processes of both metal ions and their direct proportionality with the temperature. The results of the adsorption and kinetic isotherms prove to fit the Langmuir isotherm as well as the n-order model. The adsorption reaction order for Zr and Y ions were 1.74 and 2.18, respectively. The results of thermodynamics confirmed the chemical nature of adsorption processes in addition to their endothermic properties The real experimentation of the manufactured composite was carried out on an effluent solution, where the high efficiency of recovery of the two metal ions was proved, which puts great hopes for its use as an adsorbent of zirconium and yttrium ions in the future.

Acknowledgements The author would like to express his gratitude to the collaborating members of the Nuclear Materials Authority and the Egyptian Atomic Energy Authority for their kind support in completing this work.

Author Contributions Material preparation, data collection, and analysis were performed by AAE. The draft manuscript was written by AAE, who approved the final manuscript.

Funding Open access funding provided by The Science, Technology & Innovation Funding Authority (STDF) in cooperation with The Egyptian Knowledge Bank (EKB). The author declares that no funds, grants, or other support were received during the preparation of this manuscript.

Data Availability All the data used for this work are publicly available.

Declarations

Conflict of interest The author has no relevant financial or non-financial interests to disclose.

References

1. S.A. Cotton, *Scandium, Yttrium & the Lanthanides: Inorganic & Coordination Chemistry, Encyclopedia of Inorganic Chemistry* (Wiley, New York, 2006)
2. S. Sonal, B.K. Mishra, J. Chem. Eng. **424**, 130509 (2021). https://doi.org/10.1016/j.cej.2021.130509
3. R. Leggett, J. Radiol. Prot. **37**, 434 (2017). https://doi.org/10.1088/1361-6498/aa6e66
4. S.H. Vajargah, H. Madaahhosseini, Z. Nemati, J. Alloys Compd. **430**, 339 (2007). https://doi.org/10.1016/j.jallcom.2006.05.023
5. R. Salem, R.J. Lewandowski, Clin. Gastroenterol. Hepatol. **11**, 604 (2013). https://doi.org/10.1016/j.cgh.2012.12.039
6. Y. Cho, S. Kang, Y.W. Nahm, A.Y. Mohamed, Y. Kim, D.-Y. Cho, S. Cho, ACS Omega **7**, 25078 (2022). https://doi.org/10.1021/acsomega.2c01334
7. A.V. Naumov, Russ. J. Non-Ferr. Met. **49**, 14 (2008). https://doi.org/10.1007/s11981-008-1004-6
8. S. Kuang, W. Liao, Sci. China Technol. Sci. **61**, 1319 (2018). https://doi.org/10.1007/s11431-018-9295-0
9. A.E. Mubark, S.E.A.E. Razek, A.A. Eliwa, S.M. Elgamasy, Solvent Extr. Ion Exch. (2023). https://doi.org/10.1080/07366299.2023.218618
10. H.H. El Agamy, A.E. Mubark, E.A. Gamil, N.A. Abdel-Fattah, A.A. Eliwa, Chem. Pap. (2023). https://doi.org/10.1007/s11696-023-02699-2
11. N.N. Hidayah, S.Z. Abidin, Miner. Eng. **121**, 146 (2018). https://doi.org/10.1016/j.mineng.2017.07.014
12. L.I. Deqian, J. Rare Earth. **35**, 107 (2017). https://doi.org/10.1016/S1002-0721(17)60888-3
13. F. Xie, T.A. Zhang, D. Dreisinger, F. Doyle, Min. Eng. **56**, 10 (2014). https://doi.org/10.1016/j.mineng.2013.10.021
14. L.Y. Wang, M.S. Lee, J. Ind. Eng. Chem. **39**, 1 (2016). https://doi.org/10.1016/j.jiec.2016.06.004
15. L. Xu, Y. Xiao, A. Sandwijk, Q. Xu, Y. Yang, J. Nucl. Mater. **466**, 21 (2015). https://doi.org/10.1016/j.jnucmat.2015.07.010
16. B. Mwewa, M. Tadie, S. Ndlovu, G.S. Simate, E. Matinde, J. Environ. Chem. Eng. (2022). https://doi.org/10.1016/j.jece.2022.107704
17. E.C.B. Felipe, A.C.Q. Ladeira, Sep. Sci. Technol. (2018). https://doi.org/10.1080/01496395.2017.1385624
18. X.L. Wang, L. Ye, H. Jing, Z.Z. Yu, L.L. Bo, B.L. Dong, J. Environ. Radioact. **197**, 81 (2019). https://doi.org/10.1016/j.jenvrad.2018.12.002
19. A.A. Eliwa, A.E. Mubark, Int. J. Environ. Anal. Chem. (2021). https://doi.org/10.1080/03067319.2021.1921762
20. A.A. Eliwa, E.A. Gawad, A.E. Mubark, N.A. Abel-Fattah, JOM **73**, 3419 (2021). https://doi.org/10.1007/s11837-021-04837-1
21. G.M. Abdel-Wahab, W.M. Abdellah, A.M. Yousif, A.E. Mubark, Mining. Metall. Explor. **39**, 833 (2022). https://doi.org/10.1007/s42461-019-00136-1
22. A.H. Ali, S.M. Abdo, G.A. Dakroury, Environ. Sci. Pollut. Res. **30**, 58330 (2023). https://doi.org/10.1007/s11356-023-26485-5
23. M.M. Rajmane, B.M. Sargar, S.V. Mahamuni, J. Serb. Chem. Soc. **71**, 223 (2006). https://doi.org/10.2298/JSC0603223R
24. G. Sharma, A. Kumar, M. Naushad, B. Thakur, D.V.N. Vo, B. Gao, A.A. Al-Kahtani, F.J. Stadler, J. Hazard. Mater. **416**, 125714 (2021). https://doi.org/10.1016/j.jhazmat.2021.125714
25. M.K. Jha, A. Kumari, R. Panda, J.R. Kumar, K. Yoo, J.Y. Lee, Hydrometallurgy **165**, 2 (2016). https://doi.org/10.1016/j.hydromet.2016.01.035
26. B.C. Bhatta, N. Panda, S. Mishra, Int. J. Miner. Metall. Mater. **20**, 823 (2013). https://doi.org/10.1007/s12613-013-0802-8
27. D.G. Trikkaliotis, A.K. Christoforidis, A.C. Mitropoulos, G.Z. Kyzas, Chem. Eng. (2021). https://doi.org/10.3390/chemengineering5030064
28. H. Alamgholiloo, S. Rostamnia, K. Zhang, T.H. Lee, Y. Lee, R.S. Varma, H.W. Jang, M. Shokouhimehr, ACS Omega (2020). https://doi.org/10.1021/acsomega.9b04209
29. H. Alamgholiloo, N.N. Pesyan, R. Mohammadi, S. Rostamnia, M. Shokouhimehr, J. Environ. Chem. Eng. **9**, 105486 (2021). https://doi.org/10.1016/j.jece.2021.105486

30. Z. Marczenko, M. Balcerzak, *Separation, Preconcentration and Spectrophotometry in Inorganic Analysis*, 1st edn. (Elsevier, Amsterdam, 2000), pp.140–480
31. S.I. Moussa, Z.A. Mekawy, G.A. Dakroury, A.M. Mousa, K.F. Allan, J. Polym. Environ. **31**, 2148 (2023). https://doi.org/10.1007/s10924-022-02735-4
32. M. Yadav, N.K. Singh, Appl Water Sci **7**, 4793 (2017). https://doi.org/10.1007/s13201-017-0602-9
33. G.A. Dakroury, E.A.A. El-Shazly, H.S. Hassan, Carbon Lett. **32**, 495 (2022). https://doi.org/10.1007/s42823-021-00280-z
34. A.A. Eliwa, A.E. Mubark, G.A. Dakroury, E.A.A. El-Shazly, K.M. El-Azony, J. Environ. Chem. Eng. **10**, 108886 (2022). https://doi.org/10.1016/j.jece.2022.108886
35. H.J. Kreuzer, I. Tamblyn, *Thermodynamics* (World Scientific Publishing co., Singapore, 2010), pp.209–218
36. K.V. Kumar, K. Porkodi, J. Hazard. Mater. **146**, 214 (2007). https://doi.org/10.1016/j.jhazmat.2006.12.010
37. F. Monroy-Guzman, L.V. Dsaz-Archundia, S. Hernandez-Cortés, J. Braz. Chem. Soc. **19**, 380 (2008). https://doi.org/10.1590/S0103-50532008000300003
38. X. Qiao, S. Liao, C. You, R. Chen, Catalysts **5**, 981 (2015). https://doi.org/10.3390/catal5020981
39. E. Czarnecka, J. Nowaczyk, Polym. J. **12**, 1794 (2020). https://doi.org/10.3390/polym12081794
40. B. Li, C. Wu, Y. Han, X. Ma, Z. Luo, J. Macromol. Sci. **60**, 589 (2021). https://doi.org/10.1080/00222348.2021.1887602
41. M. Buchholz, I. Spahn, B. Scholten, H.H. Coenen, Radioch. Acta. **101**, 491 (2013). https://doi.org/10.1524/ract.2013.2083
42. M.T. Colomer, J. Sol-Gel Sci. Technol. **67**, 135 (2013). https://doi.org/10.1007/s10971-013-3059-9
43. M.M. Rajmane, B.M. Sargar, S.V. Mahamuni, M.A. Anuse, J. Serb. Chem. Soc. **71**, 223 (2006). https://doi.org/10.2298/JSC0603223R
44. N. Yasir, A.S. Khan, N. Akbar, M.F. Hassan, T.H. Ibrahim, M. Khamis, R. Siddiqui, N.A. Khan, P. Nancarrow, Processes **10**, 794 (2022). https://doi.org/10.3390/pr10040794
45. G.F. Oliveira, R.C. Andrade, M.A.G. Trindade, H.M.C. Andrade, C.T. Carvalho, Biomass Source Babassu. (2017). https://doi.org/10.21577/0100-4042.20160191
46. A. Ahmed, A. Singh, S.J. Young, V. Gupta, M. Singh, S. Arya, Composites A **165**, 107373 (2023). https://doi.org/10.1016/j.compositesa.2022.107373
47. E.K. Radwan, H. Kafafy, S.T. El-Wakeel, T.I. Shaheen, T.A. Gad-Allah, A.S. El-Kalliny, M.E. El-Naggar, Cellular **25**, 6645 (2018). https://doi.org/10.1007/s10570-018-2003-0
48. L. Xu, J. Zhang, J. Ding, T. Liu, G. Shi, X. Li, W. Dang, Y. Cheng, R. Guo, J. Miner. **10**, 72 (2020)
49. M. Andrianainarivelo, Int. J. Mater. Chem. **10**, 1 (2020). https://doi.org/10.5923/j.ijmc.20201001.01
50. Y. Jiaoa, D. Hanb, Y. Lua, Y. Ronga, L. Fanga, Y. Liua, R. Han, Desalin. Water Treat. **77**, 247–255 (2017). https://doi.org/10.5004/dwt.2017.20780
51. E. Igberase, P. Osifo, A. Ofomaja, Int. J. Anal. Chem. (2017). https://doi.org/10.1155/2017/6150209
52. K. Dae-Joon, H. Sang-Hoon, K. Seung-Goo, Y. Masatomo, J. Am. Ceram. Soc. (1994). https://doi.org/10.1111/j.1151-2916.1994.tb07035.x
53. https://bcs.whfreeman.com/WebPub/Chemistry/raynercanham6e/Appendices/Rayner-Canham%205e%20Appendix%202%20-%20Charge%20Densities%20of%20Selected%20Ions.pdf
54. K.Y. Foo, B.H. Hameed, J. Chem. Eng. **156**, 2 (2010). https://doi.org/10.1016/j.cej.2009.09.013
55. G.A. Dakroury, S.M. Ali, H.S. Hassan, J. Polym. Res. **28**, 385 (2021). https://doi.org/10.1007/s10965-021-02753-1
56. A.N. Spiess, N. Neumeyer, BMC Pharmacol. (2010). https://doi.org/10.1186/1471-2210-10-6
57. A.A. Eliwa, Int. J. Environ. Anal. Chem. (2022). https://doi.org/10.1080/03067319.2022.2116980
58. H. Lü, H. An, Z. Xie, Int. J. Biol. Macromol. **56**, 89 (2013). https://doi.org/10.1016/j.ijbiomac.2013.02.003
59. Y.M. Khawassek, A.A. Eliwa, E.A. Gawad, S.M. Abdo, J. Radiat. Res. Appl. Sci. **8**, 583 (2015). https://doi.org/10.1016/j.jrras.2015.07.002
60. A. Merikhy, A. Heydari, H. Eskandari, F. Ghahraman-Rozegar, Chem. Eng. Process. **158**, 108167 (2020). https://doi.org/10.1016/j.cep.2020.108167
61. R. Bai, F. Yang, L. Meng, Z. Zhao, W. Guo, C. Cai, Y. Zhang, Mater. Des. **197**, 109195 (2021). https://doi.org/10.1016/j.matdes.2020.109195
62. M.F. Cheira, M.N. Kouraim, I.H. Zidan, W.S. Mohamed, T.F. Hassanein, J. Environ. Chem. Eng. **8**, 104427 (2020). https://doi.org/10.1016/j.jece.2020.104427
63. A.K. Sakr, M.F. Cheira, M.A. Hassanin, H.I. Mira, S.A. Mohamed, M.U. Khandaker, H. Osman, E.M. Eed, M.I. Sayyed, M.Y. Hanfi, J. Appl. Sci. **11**, 10320 (2021). https://doi.org/10.3390/app112110320
64. M.A. Zulfikar, R. Zarlina, Rusnadi, N. Handayani, A. Alni, D. Wahyuningrum, Russ. J. Non-Ferr. Met. **58**, 614 (2017)
65. D. Kong, E. Kusrini, L.D. Wilson, Micromachines **12**, 478 (2021). https://doi.org/10.3390/mi12050478
66. E.C.B. Felipe, H.G. Palhares, A.C.Q. Ladeira, Separation of zirconium from hafnium by ion exchange (International Nuclear Atlantic Conference Brazil, 2013), https://inis.iaea.org/collection/NCLCollectionStore/_Public/45/075/45075421.pdf
67. A.M. Donia, A.A. Atia, A.M. Daher, E.A. Elshehy, J. Dispers. Sci. Technol. **32**, 193 (2011). https://doi.org/10.1080/01932691003656730
68. W. Qin, S. Xu, G. Xu, Q. Xie, C. Wang, Z. Xu, J. Chem. Eng. **225**, 528 (2013). https://doi.org/10.1016/j.cej.2013.03.127
69. A. Das, K.R.S. Chandrakumar, B. Paul, S.M. Chopad, S. Majumdar, A.K. Singh, V. Kain, Sep. Purif. Technol. (2020). https://doi.org/10.1016/j.seppur.2020.116518
70. A.M. Donia, A.A. Atia, A.M. Daher, O.A. Desouky, E.A. Elshehy, Sep. Sci. Technol. **46**, 1 (2011). https://doi.org/10.1080/01496395.2011.558036